Perspective

Cite This: Biomacromolecules 2018, 19, 1469−1484

pubs.acs.org/Biomac

Distributions: The Importance of the Chemist's Molecular View for Biological Materials

Rachel L. Merzel,[†] Bradford G. Orr,[‡] and Mark M. Banaszak Holl*[,§]

[†]Department of Chemistry and [‡]Department of Physics, University of Michigan, Ann Arbor, Michigan 48109, United States
[§]Chemical Engineering, Monash University, Clayton, Victoria 3800, Australia

ABSTRACT: Characterization of materials with biological applications and assessment of physiological effects of therapeutic interventions are critical for translating research to the clinic and preventing adverse reactions. Analytical techniques typically used to characterize targeted nanomaterials and tissues rely on bulk measurement. Therefore, the resulting data represent an *average* structure of the sample, masking stochastic (randomly generated) distributions that are commonly present. In this Perspective, we examine almost 20 years of work our group has done in different fields to characterize and control distributions. We discuss the analytical techniques and statistical methods we use and illustrate how we leverage them in tandem with other bulk techniques. We also discuss the challenges and time investment associated with taking such a detailed view of distributions as well as the risks of not fully appreciating the extent of heterogeneity present in many systems. Through three case studies showcasing our research on conjugated polymers for drug delivery, collagen in bone, and endogenous protein nanoparticles, we discuss how identification and characterization of distributions, i.e., a molecular view of the system, was critical for understanding the observed biological effects. In all three cases, data would have been misinterpreted and insights missed if we had only relied upon spatially averaged data. Finally, we discuss how new techniques are starting to bridge the gap between bulk and molecular level analysis, bringing more opportunity and capacity to the research community to address the challenges of distributions and their roles in biology, chemistry, and the translation of science and engineering to societal challenges.

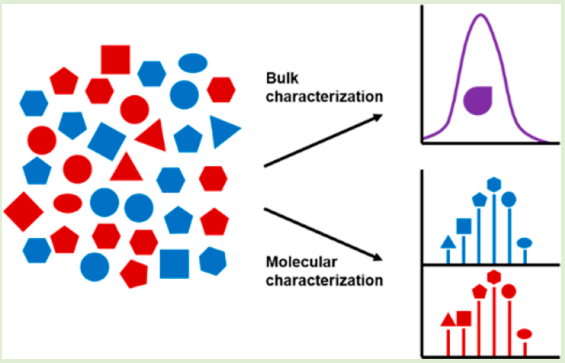

INTRODUCTION

Characterization of Nanomaterials and Nanostructures in Biology. In this Perspective, we consider nearly 20 years of effort in our group to characterize stochastic (randomly occurring) distributions arising from molecular level chemistry in a variety of synthetic and natural systems. As a research team composed primarily of chemists, engineers, and physicists with highly integrated medical collaborators and mentors, our group brings distinct perspectives and expertise to characterizing biological materials. Generally, the extent of heterogeneity and the role material distributions play has not been fully appreciated. Here, we present three case studies in the arenas of targeted drug delivery and tissue analysis illustrating the importance of a molecular view of biomaterials and the specific contributions of our research to these fields. Specifically, we highlight examples of how detailed characterizations, and sometimes intentional removal, of distributions have proven critical to understanding biological behavior.

Analytical Techniques for Nanoscale Characterization. Most analytical techniques used to characterize nanoscale materials and nanostructures rely on bulk measurement. That is, they average over a much larger length scale than the constitutive molecules or nanomaterials. The resulting data represent an *average* molecular and/or nanoscale structure of the sample. For example, conventional spectroscopic techniques (e.g., NMR, IR, UV−vis), X-ray diffraction (XRD), and dynamic light scattering (DLS) contain information regarding the distribution of the sample with line-widths that are not simply interpreted and are often convolved with other physical properties. The bulk characterization masks stochastic distributions present within the biological nanomaterials. If a new targeted nanoscale therapy comprises a stochastic distribution, it is difficult, if not impossible, to know which species produced the observed physiological effect. In biological tissues, e.g., bone and skin, most characterization techniques hide natural heterogeneity or mask localized changes to micro- and nanostructure as a result of disease or therapeutic intervention because the analysis averages over micrometers to millimeters or even greater sample dimensions. Precise characterization of nanoscale materials and anatomical changes is critical to developing safe and targeted therapies as well as understanding their physiological effects.[1]

Molecular level characterization of samples and elucidation of structure are a challenging problem. In the research presented here, we primarily took advantage of two techniques to characterize and/or control distributions: reverse-phase high performance liquid chromatography (rp-HPLC) and atomic

Received: March 2, 2018
Revised: April 15, 2018
Published: April 17, 2018

DOI: 10.1021/acs.biomac.8b00375
Biomacromolecules 2018, 19, 1469−1484

force microscopy (AFM). We complemented these methods with other bulk techniques, notably NMR and fluorescence spectroscopy, mass spectrometry, DLS, confocal microscopy, and fluorescence lifetime imaging microscopy (FLIM). We demonstrated that rp-HPLC can be used to separate trailing and branching defects in poly(amidoamine) (PAMAM) dendrimers[2−5] and separate species with different numbers of hydrophobic ligands (dyes, drugs, targeting agents) attached to the hydrophilic backbone.[6−10] AFM allowed for direct, representative imaging of samples and surfaces with nanometer precision in the x and y directions and subnanometer precision vertically.[11−21] Importantly, AFM is a topographic technique, measuring the volume of imaged features along with surface morphology and material properties. Hierarchical features from the nanometer to micron scale can be characterized, and no staining is required for contrast.[15] The large number of individually characterized nanostructures in each AFM image enables robust statistical analysis.

Researchers also turn to XRD because it can provide high resolution (subangstrom) information with structural information down to the molecular level. However, these values are calculated from combined measurements of a large sample set of molecules throughout the bulk material: micrometers to millimeters in the crystal. Crystal structures obtained by XRD represent a spatial average and tend to treat molecular differences as "disorder," masking heterogeneity in the sample. Conversely, AFM typically produces images with slightly lower resolution but provides particle-by-particle measurements. This molecular level analysis is critical for assessing distributions in biological materials and relating changes in distributions to activity.

In our research, we use molecular level and bulk techniques together to build greater scientific understanding. We take advantage of image processing software—particle counting, alignment mapping, and so forth—to process large data sets with thousands of structures. We also use conventional cellular biology techniques such as confocal microscopy and flow cytometry to probe the biological implications of distributions. In sum, we make the case here for the investment in a molecular level analysis of biological materials and the importance of understanding the interplay between structural variation and function.

Three Cases for a Molecular View in Biological Materials. In the rest of this Perspective, we present three broad research studies illustrating the role distributions play in assessing biological materials and outcomes. The first section focuses on multivalent polymers as drug delivery vectors, specifically the challenges associated with heterogeneity resulting from sequential stochastic conjugations. The second section discusses inherent heterogeneity in tissue and changes to the hierarchical structure of collagen as functions of disease and drug treatment. In the third section, we return to drug delivery and combine our analyses of distributions in artificial and natural materials. We highlight our latest research on serum proteins and the role they play in trafficking and bioidentity of their ligands. Analyses of distributions of serum protein nanoparticles (aggregated protein) as functions of concentration and ligand identity yielded novel hypotheses on the relationship between protein aggregation and activity. This was particularly important for understanding the role of serum proteins in the trafficking of the multivalent polymers discussed in the first section. We emphasize how the success of this work depended on applying lessons on conjugation heterogeneity and collagen characterization from the first two research cases. We translated our understanding of material distributions derived from laboratory synthesis processes and inherently present in natural materials as well as our expertise in AFM and image analysis to exploring the relationship among structure, function, and activity in protein nanoparticles. In all three cases, we demonstrate how key insights and conclusions would have been missed if we had only used techniques that measure over larger scales than the molecules or nanostructures in the biological materials.

Distributions in Targeted Nanoparticles. *History and Motivation.* Over almost 20 years, our group and close collaborators have invested substantial research effort toward developing targeted therapeutics on a generation 5 (G5) PAMAM dendrimer scaffold.[6−9,22−34] In the mid-2000s, our colleagues developed a targeted dendrimer cancer therapeutic that demonstrated significant toxicity to tumor cells in vitro.[30] The targeted dendrimer was cleared for Phase I clinical trials. However, sufficient quantities for a clinical trial (kilograms) could not be manufactured consistently, and the trial never moved forward. Much of our work since that time has been aimed at trying to understand the challenges in scientific understanding, material processing and scale-up, and clinical translation that arise when a small number of ligands is conjugated to a comparatively large number of attachment sites.[2−10] Note that G5 PAMAM has a theoretical 128 attachment sites (purified G5 PAMAM monomer, discussed below, has an average of 93 attachment sites).[4]

In general, nanomaterials (particles, polymers, metals, micelles, etc.) have been a popular focus of research in biomedical applications, including targeted therapy, imaging, and diagnostics.[35] The ability to attach multiple copies of ligands allows for enhanced multivalent targeting and increased drug payloads. The size of the materials enables them to escape renal filtration and facilitates longer blood circulation times, increasing the chances they will reach the target tissues (G5 PAMAM is ∼5 nm in diameter). The enhanced permeability and retention (EPR) effect in leaky tumor vasculature is widely believed to contribute to increased therapeutic efficacy.[36,37] These attractive advantages have continued to make multivalent nanomaterials a popular area of biomedical research.[26,35,38−50]

Heterogeneity in Conjugated Nanomaterials. Translation to the clinic of targeted multivalent nanomaterials has been difficult. Targeted nanomaterials that perform well in vitro often cannot be formulated on large scales or exhibit unexpected side effects and toxicity when tested in vivo. We postulate that many of these adverse effects arise from highly heterogeneous mixtures resulting from multiple ligand conjugations.[10] Here, we provide brief context to highlight the scope of the challenge in creating homogeneous conjugated nanomaterials, but a full accounting of these synthetic and characterization efforts is not the focus of this Perspective. Our group has already published extensively on this work, as well as our research on characterizing, controlling, and eliminating heterogeneous distributions, in this journal[10,51] and others.[2−8,11,12] Here, we highlight a case in which we demonstrated in vitro the importance of explicit consideration of distributions in biological nanomaterials.[9]

The arithmetic mean is the most commonly used parameter for characterizing the number of (functional) ligands on a nanomaterial. Usually, this value is determined by bulk characterization such as NMR spectroscopy or gel permeation chromatography (GPC). The mean value fails to convey that the sample actually contains material with a distribution in the number of conjugated ligands. The conjugate distribution is binomial if the attachment of ligands is identical and independent

DOI: 10.1021/acs.biomac.8b00375
Biomacromolecules 2018, 19, 1469−1484

of previous binding events. If the mean number of conjugated ligands is small (e.g., three drugs or four targeting agents) and the ratio of reacted sites to total initial number of sites is low compared to the number of attachment sites (e.g., 128 in a G5 PAMAM dendrimer), the distribution is Poissonian as opposed to Gaussian.[52,53] Characterization of nanomaterials subjected to sequential conjugations (e.g., a targeting agent and then a drug) is more complicated still because the distributions are multiplicative.[2,3,10]

Consider a PAMAM dendrimer conjugate with a mean of four targeting folic acid (FA) and five therapeutic methotrexate (MTX). Figure 1a shows the distribution of species if only four

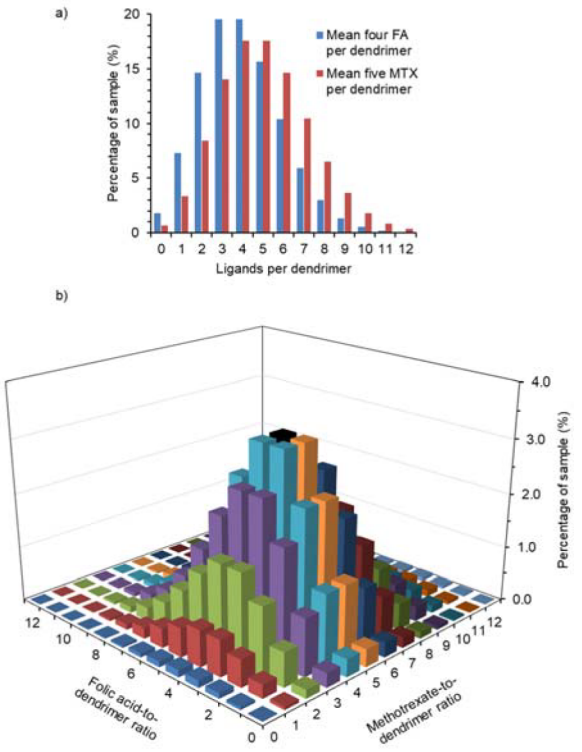

Figure 1. (a) Poisson distributions of stochastic mixtures of dendrimers with an average of four or five ligands. (b) Distribution of species resulting from sequential conjugation of averages of four then five ligands. The chart represents the product of the two distributions. The black bar indicates the nominal material with four FA and five MTX.

FA or five MTX were conjugated to the dendrimer. Figure 1b demonstrates the multiplicative effect of combining two Poisson distributions resulting from stochastic reaction conditions. At most, 3−4% of the doubly conjugated sample material contains four FA and five MTX ligands. This does not take into account differences in reactivity between the ligands, site-blocking effects with increasing number of ligands conjugated, or autocatalysis of the conjugation process. All these factors can increase the heterogeneity of the system and further decrease the concentration of the mean material. In many cases, the nominal "average" material may comprise less than one percent of the sample. As a result, it is difficult, if not impossible, to accurately assess the nanomaterial's properties and activity, which are particularly important in biological applications. If these samples are tested for their therapeutic properties in vitro or in vivo, one or many of the species present may contribute to the observed effects. Sample heterogeneity greatly complicates research on the mechanisms of action and side effects, as well as efforts to reproduce results and translate multivalent nanomaterials to the clinic.

Heterogeneity in the scaffold itself is another factor to be considered. Our group has invested significant effort in characterizing and removing trailing generations and branching defects from commercial G5 PAMAM (Figure 2a).[4,5] Our

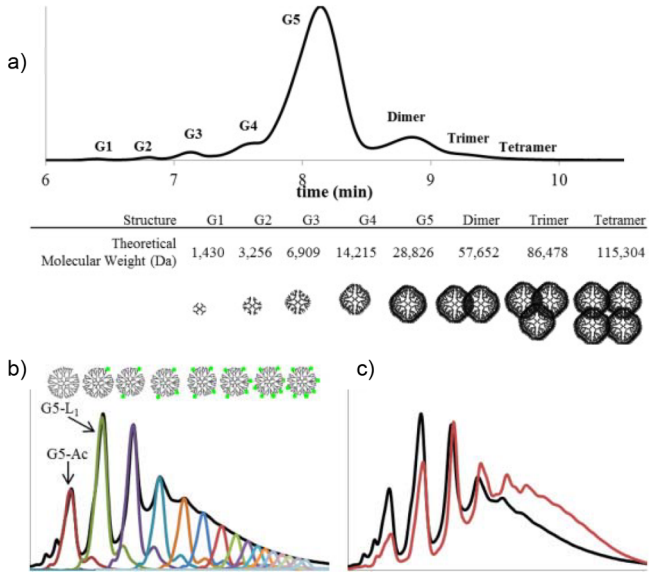

Figure 2. Ultraperformance liquid chromatography (UPLC) chromatograms at 210 nm. (a) As-received G5 dendrimer indicates the presence of trailing generation impurities as well as aggregation defects. (b) As-received acetylated G5 PAMAM (G5-Ac, red trace) contains high weight impurities with no ligand that coelute with G5 monomers containing one ligand (G5-L1, green trace) in a conjugated sample (black trace). (c) Conjugation to an rp-HPLC-purified G5 monomer sample (red trace) has narrowed peak width and improved peak resolution compared to those of the as-received conjugation (black trace). Adapted and reprinted from ref 4. Copyright 2013, with permission from Elsevier.

standard operating procedure is to purify commercially purchased G5 PAMAM to G5 monomer before using it in conjugation reactions. If we do not take this extra step, shifts induced on the rp-HPLC column by each hydrophobic ligand will not be larger than the peak width of the mass distribution of the dendrimer (Figure 2b,c and Figure 3).[4,5,10] Even with G5 PAMAM monomer, techniques such as MALDI-TOF-MS are of limited use because the mass shift is much narrower than the dendrimer mass distribution itself, and the shot noise in the mass spectrometry measurement is approximately the same as the ligand mass.

This brief background on nanomaterial−ligand distributions illustrates the scope of the challenge in designing targeted therapeutics exclusive to issues such as toxicity and biodegradability. In this context, the next subsection discusses work from our group in which we demonstrated that the number of ligands determined outcome in vitro, highlighting the critical need for appreciation and consideration of heterogeneous distributions.

Cellular Uptake and Fluorescence Change with Dye−Dendrimer Ratio (Highlighting Results from Ref 9). This study was designed to examine the differences in activity between dendrimers with precise numbers of dyes and stochastic mixtures of material. In particular, we wanted to assess the implications of using fluorescence to probe cellular uptake and localization. Understanding the interaction between the dendrimer and dye

DOI: 10.1021/acs.biomac.8b00375
Biomacromolecules 2018, 19, 1469−1484

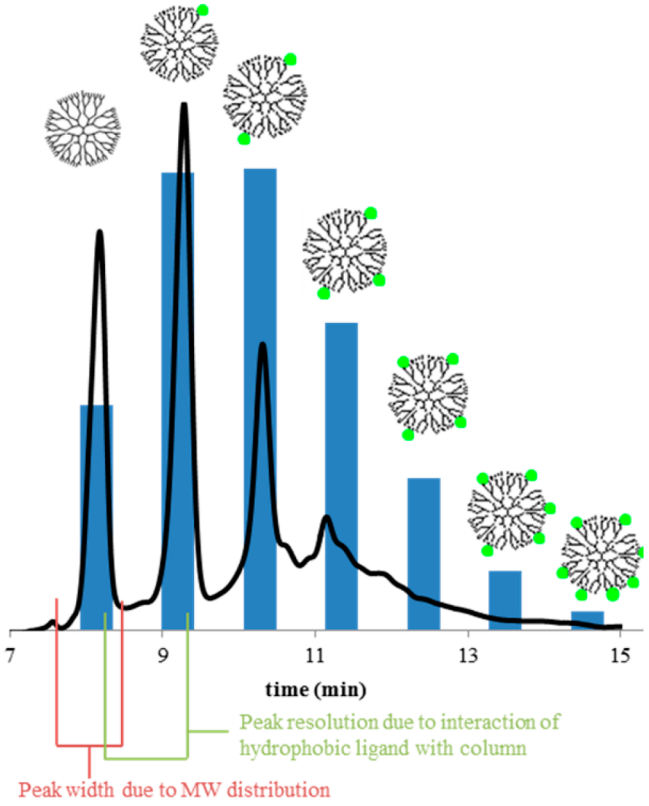

Figure 3. HPLC chromatogram of an average conjugate overlaid with the predicted distribution for an average of two ligands per particle. Reproduced with permission from ref 10. Copyright 2014, American Chemical Society.

and their response to cellular uptake is critical because the dendrimers are used as vectors for oligonucleotides, antibacterial agents, and drugs.[45,48,54−56] Fluorescent dyes are often attached to assess uptake and examine localization within cells.[57]

We prepared three categories of G5 PAMAM dendrimers conjugated to TAMRA dyes: (1) dendrimers with precisely one to four dyes attached, (2) dendrimers with five or more dyes attached, and (3) dendrimers containing a Poisson distribution of dye with an arithmetic mean of 1.5 (Scheme 1). This last material consisted of a mixture of dendrimers with 0, 1, 2, 3, 4, and 5 dyes at 22, 34, 25, 13, 5, and 1%, respectively. The solution fluorescence properties (intensity and lifetime) of the free dye and each of the six conjugates were examined in aqueous solutions and biologically relevant control solutions (e.g., cell lysate, with albumin, and in blood serum). We demonstrated that intensity increased and fluorescence lifetime decreased with increasing numbers of dyes (n), but these relationships were not linear. Confocal microscopy experiments showed that cellular uptake of the conjugates varied as a function of n. It was necessary to apply correction factors determined from the solution experiments to accurately quantify the extent of uptake. The raw mean fluorescence intensities suggested that uptake decreased with $n \geq 2$. However, once the corrections were applied, the data showed that cells took up more dendrimers with $n \geq 2$ than $n = 1$ material, the opposite trend of what the raw data indicated. The in vitro fluorescence properties of the stochastic material ($n = 1.5_{avg}$) are more complicated. Biodistribution can be affected by hydrophobicity, and material with different numbers of ligands can be "separated," or fractionated, through interactions with biomolecules.[58−61] Accurate determination of uptake would require knowing the number of conjugated dyes per dendrimer (or hydrophobic ligands per polymer more generally), the fluorescent properties of the conjugates, and which species are preferentially taken up. Application of the corrections showed that the mean fluorescence data for the stochastic mixtures had errors of at least 3- to 5-fold. Relative brightness in confocal microscopy fluorescence images cannot be relied upon to interpret cellular uptake without knowledge of the number of dyes per dendrimer. Caution is necessary when quantifying uptake of stochastic mixtures using mean fluorescence data.

FLIM experiments further emphasize this point. FLIM measurements are generally insensitive to changes in intensity but do depend on environmental conditions such as pH, ion concentration, and interactions with biomolecules.[62] We postulated that changes in lifetime due to microenvironment would allow for investigation of internal cellular structures and would be small compared to differences in lifetime resulting from variation in the dye-to-dendrimer ratio. We measured fluorescence lifetime both in cells (Figure 4a−h) and in biologically relevant control environments. In both cases, we found that changes in lifetime were of similar magnitude whether the dye ratio or the environment was held constant. The $n = 1$ and $n = 5+$ dendrimers had the longest lifetimes in cells, a phenomenon that was duplicated in control solutions (Figure 4k). Surprisingly, the $n = 1.5_{avg}$ mixture had the lowest lifetime and did not show any of the high lifetime components observed in the other high lifetime materials even though 34% of the stochastic mixture comprised the $n = 1$ dendrimer. These data show that lifetime alone cannot be used to interpret biological microenvironments if the precise number of dyes per dendrimer is not known, a situation made even more complicated if the sample has been biologically fractionated.

Overall, these results illustrate the complications associated with testing stochastic mixtures of conjugated polymers for targeted therapy or for probing intracellular structure. The fluorescence properties alone obtained from stochastic mixtures are not reliable measures of uptake or localization in a cell. Differences in the distribution from batch to batch may also change observed outcomes. Appreciation of the challenges imposed by stochastic mixtures is critical for developing new therapies, understanding their biological effects and mechanisms of action, and facilitating their translation into the clinic.

Distributions in Collagen Structure. In the first case study, we discussed distributions in artificial materials (multivalent polymer conjugates) generated for biological applications. This second case illustrates the inherent nature of material distribution in tissue, specifically collagen in bone. Our knowledge of statistical methods for studying distributions from our work on multivalent polymer conjugates translated to our research on tissue, but we also developed new methods for characterizing distributions of natural nano- and microstructures imaged by AFM.

Type I collagen is the most abundant protein in the body, and therefore, detailed understanding of collagen structure is critical for assessing the effectiveness and impact of a wide variety of diseases and treatments.[63−67] Our group has studied naturally occurring distributions over multiple levels of the hierarchical nature of collagen (Figure 5). The work presented here summarizes our efforts to characterize distributions of repeating nanoscale features resulting from the packing of collagen molecules and microstructure and alignment of collagen fibers. We explore the relationship between changes to collagen nano-

DOI: 10.1021/acs.biomac.8b00375
Biomacromolecules 2018, 19, 1469−1484

Scheme 1. Synthesis, Isolation, and Characterization of G5-NH2-TAMRAn (n = 0, 1, 2, 3, 4, 5+, 1.5 avg) Samples: (a) Stochastic Conjugation of TAMRA to G5 PAMAM Dendrimer, (b) Isolation of G5-NH2-TAMRAn Employing Semipreparative rp-HPLC, and (c) Reinjection of Combined Fractions on Analytical rp-UPLC to Determine Purity[a]

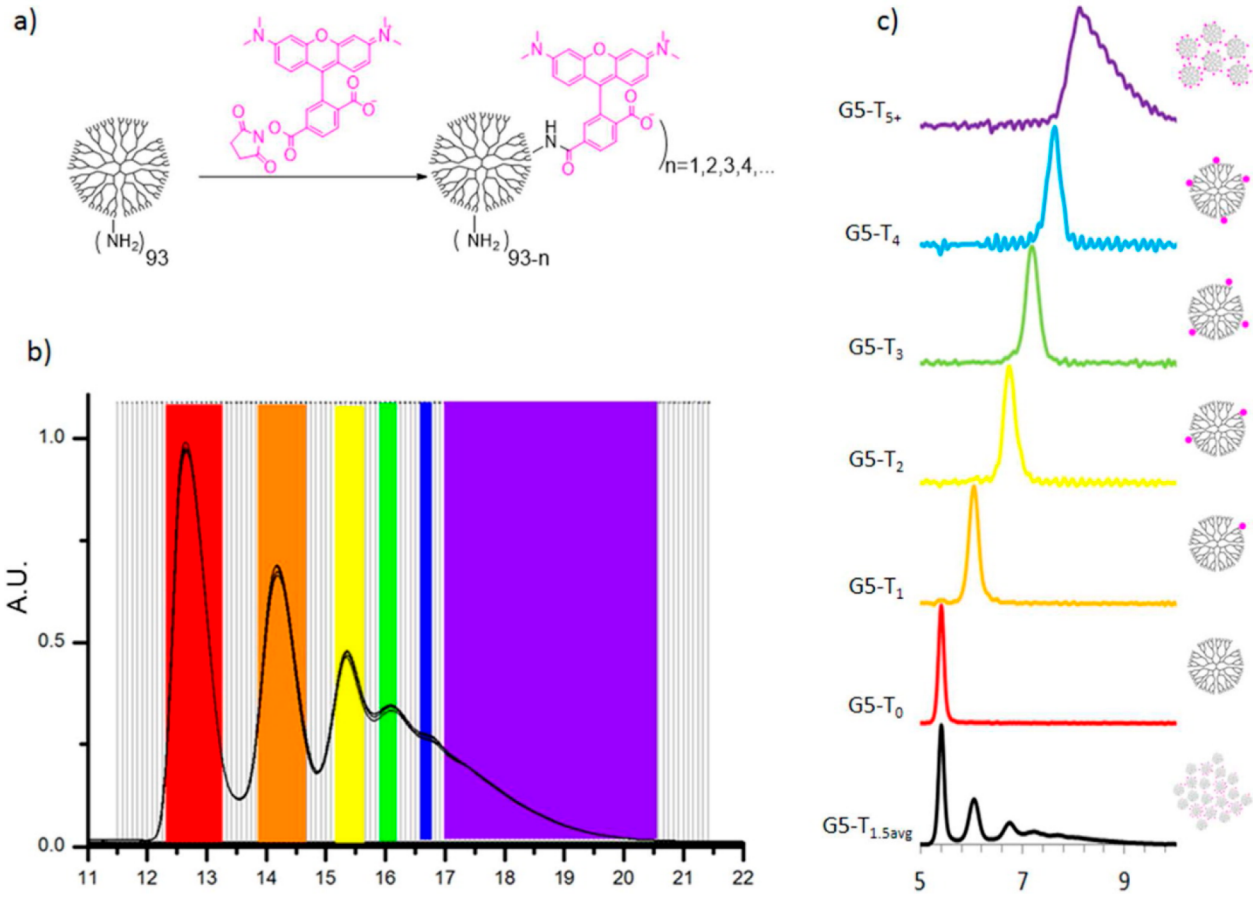

Reproduced with permission from ref 9. Copyright 2015, American Chemical Society. [a]n = 1.5 avg (black), 0 (red), 1 (orange), 2 (yellow), 3 (green), 4 (blue), and 5+ (purple).

and microstructure as functions of bone type, disease (osteoporosis induced by estrogen depletion), and treatment. We emphasize how macroscopic analysis methods fail to detect changes in collagen architecture that contribute to the inherent heterogeneity in collagenous tissue.

A Brief Introduction to Collagen. Type I collagen forms the structural scaffold bones, dentin, skin, and tendon.[63−67] As illustrated in Figure 5, Type I collagen assembles into hierarchical structures, forming microfibrils, fibrils, fibers or bundles, and tissues.[14−19,66−78] Various models have been proposed for fibril assembly and the origin of *D*-spacing. In 1963, the Hodge Petruska model depicted the collagen molecules parallel to each other but staggered, resulting in a repeating gap/overlap pattern that gave rise to the single 67 nm *D*-spacing value.[68] According to the Orgel model for fibril assembly, five microfibrils (each composed of three collagen molecules twisted in an α-helix) are packed quasi-hexagonally in the equatorial plane and super-twisted axially.[69] This is a 3D model for fibril assembly based on XRD studies. Both the Hodge Petruska and Orgel models require a single value for the *D*-spacing of type I collagen, which is commonly reported as 67 nm calculated from XRD, EM, or computational models of the collagen molecule. Each of these techniques provides an average representation of the structure.

Conversely, our group has focused on a fibril-by-fibril approach to collagen analysis. Using AFM, we acquired images across heterogeneous tissue surfaces (bone, skin, tendon, and tail from sheep, rats, rabbits, and monkeys) to obtain representative data sets containing thousands of fibrils.[13−20] We then quantified the *D*-spacing on a fibril-by-fibril basis using two-dimensional fast Fourier transform (2D FFT) analysis. The inclusion of thousands of fibrils allowed for statistically robust analyses. We have demonstrated non-Gaussian distributions in collagen nanomorphology with *D*-spacing measured from 59 to 75 nm.[13−20] We found that, in general, there is very little variation in *D*-spacings within bundles (groups of aligned fibrils) but large variations between bundles.[18] Existing models of collagen structure cannot explain these *D*-spacing distributions, but a recent study documented changes in collagen structure at all levels of hierarchy, including *D*-spacing, as a function of disease.[67] Nevertheless, the formation and assembly of collagen fibrils affect the properties of the tissue. Research is still ongoing to understanding the physiological processes, mechanical stresses, and diseases that affect the distributions of *D*-spacings.

Fibril-by-Fibril and Multimicrometer Approaches (Highlighting Results from Refs 20 and 21). In more recent work, we have developed methods for hand-coding the alignment of collagen fibrils (Figure 6).[20] We documented surface heterogeneity and changes in collagen microstructure that would not be reflected in average values incorporating measurements from many fibrils over a larger area of the tissue surface.

DOI: 10.1021/acs.biomac.8b00375
Biomacromolecules 2018, 19, 1469−1484

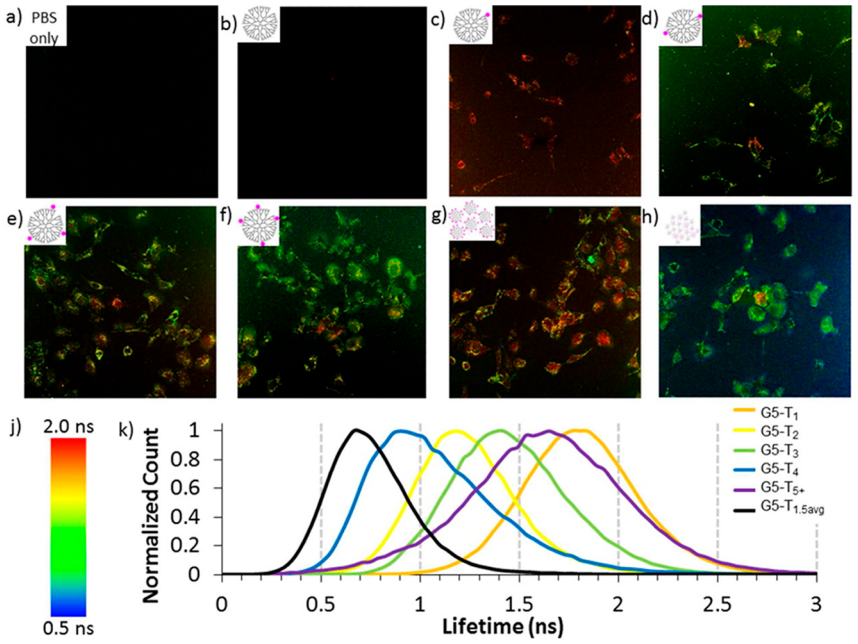

Figure 4. FLIM images of HEK293A cells incubated for 3 h with (a) PBS only, (b) G5-NH_2, (c) G5-NH_2-$TAMRA_1$, (d) G5-NH_2-$TAMRA_2$, (e) G5-NH_2-$TAMRA_3$, (f) G5-NH_2-$TAMRA_4$, (g) G5-NH_2-$TAMRA_{5+}$, and (h) G5-NH_2-$TAMRA_{1.5avg}$. (j) Color code for FLIM images. (k) Histograms of fluorescence lifetimes for FLIM images. Images were obtained with a 40× oil immersion objective. Reproduced with permission from ref 9. Copyright 2015, American Chemical Society.

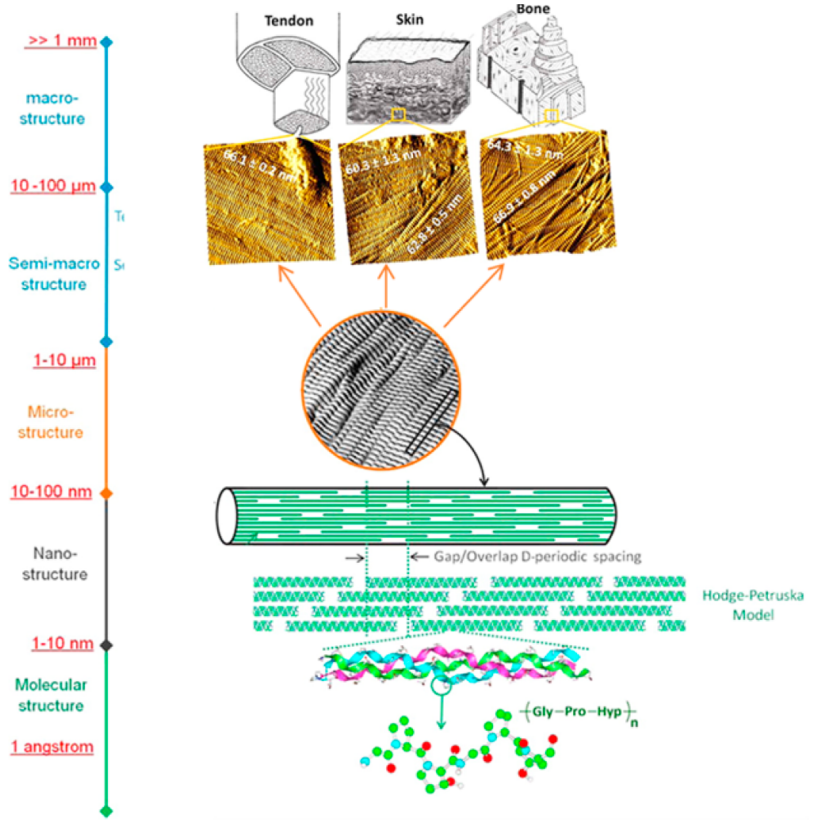

Figure 5. Hierarchical structure of collagen structures in tendon, skin, and bone. The AFM images show the *D*-spacing resulting from the parallel staggered alignment of the collagen microfibrils. Reproduced with permission from ref 18. Copyright 2012, American Chemical Society.

Here, we highlight a case in which microstructures changed as a function of disease, estrogen depletion modeling osteoporosis, and treatment with three different drugs. In sum, the study involved analyzing a total of 5,673 fibrils from 84 rabbits split into seven treatment groups.[20,21] After ovariectomy-induced estrogen depletion, the osteoporosis drugs were given to the rabbits as a preventive, not as treatment. Note that all the imaging and analysis was carried out blind to the identity of the samples.

DOI: 10.1021/acs.biomac.8b00375
Biomacromolecules 2018, 19, 1469−1484

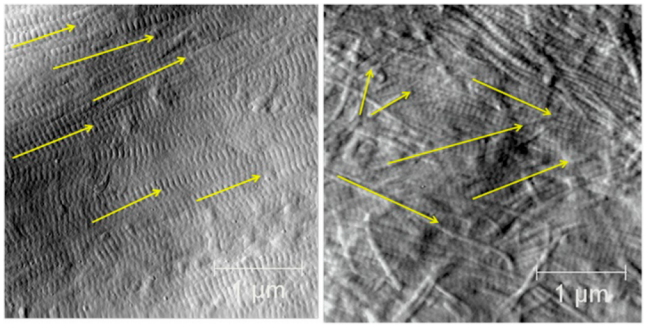

Figure 6. AFM images illustrating parallel and oblique regions of Type I collagen fibrils. (a) Parallel region showing multiple aligned fibrils (yellow arrows); (b) oblique region showing multiple fibrils with varying alignment (yellow arrows). Reproduced with permission from ref 20. Copyright 2015, Nature Springer.

Microstructures in the images were hand-coded as bundles if 3–15 fibrils aligned in the same direction and were associated with one another and sheets if more than 20 fibrils aligned in the same direction and were continuous with surrounding bone. Together, bundles and sheets were considered to contain *parallel* fibrils, and nonaligned fibrils were *oblique* (Figure 6). This coding scheme captured at least 95% of all the measured fibrils.

Importantly, changes to collagen microstructures were observed in cortical bone (compact bone that makes up the long bones, e.g., femur) but not in trabecular bone ("spongy" bone that remodels faster than cortical bone, e.g., the interior of vertebrae) (Figure 7). In the control cortical bone, estrogen

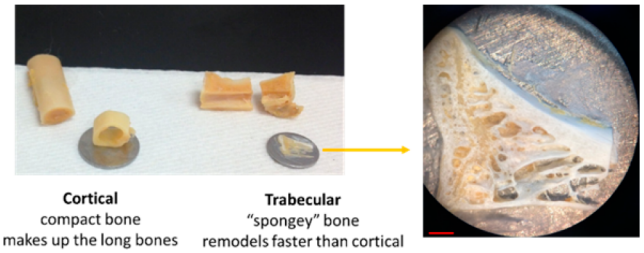

Figure 7. Examples of cortical and trabecular bone. Left image courtesy of Meagan Cauble. Right image reprinted from ref 21. Copyright 2016, with permission from the authors.

depletion caused a statistically significant change in the proportions of parallel and oblique fibrils: incidence of parallel fibrils decreased and oblique fibrils increased. In the treated animals, the two drugs currently in the clinic partially prevented this change, and the experimental drug fully prevented it.

In both trabecular and cortical bone, the mean *D*-spacing value and the overall *D*-spacing distributions did not change with treatment. In bundles, no significant differences existed between the groups (Figure 8). However, treatment induced significant animal-to-animal variability in bundle *D*-spacing in trabecular bone. That is, the *D*-spacing means and distributions in trabecular bone remained the same, but *D*-spacings in trabecular bundles were different from animal-to-animal. The control rabbits displayed zero variability (including incorporation of a random effect for the animal) in their bundle distributions; ovariectomized rabbits had nonsignificant animal-to-animal variability, and the two treatment groups both had significant variability. The phenomenon was not observed in cortical bone. As trabecular bone is responsible for bone growth and remodeling, changes to trabecular collagen structure is of consequence.

More generally, these results provide important insights on the range of reactions to therapies. The differences in response and outcome will likely be even more pronounced in more genetically diverse populations, e.g., humans. These trends would have been missed if employing techniques that only capture the arithmetic mean of *D*-spacing values averaged over micro- to millimeters (such as XRD); all values would have been the same, and no information regarding the drug effects would have been obtained.

Given the time and labor investment necessary for hand-coding fibril alignment, we sought ways to accelerate and streamline the process. With collaborators, we developed an autocorrelation approach to recognize patterns and quantitatively assess the degree of fibril alignment.[21] The full image level analysis (Figure 9) generates vector fields that mathematically approximate collagen fibril alignment. These vector fields were used to compute an information-theoretic entropy value: a fibril alignment parameter (FAP). We applied this approach to assessing fibril alignment in cortical and trabecular bone in estrogen-depleted and -treated animals. FAP distributions showed trabecular fibril alignment shifting toward cortical FAP distributions after ovariectomy. In cortical bone, estrogen depletion affected the formation of bundles and sheets. The three drugs examined affected alignment in cortical and trabecular bone differently. In one case, the drug moved FAP distributions in opposite directions in cortical and trabecular bone. The ability to quickly obtain fibril alignment information across a multimicrometer scale is important. Together, *D*-spacing analysis, hand coding of microstructures, and the FAP distributions provide data on multiple levels of the collagen hierarchical structures, which are critical for understanding and treating disease.

Implications for Treatment of Bone Diseases. The research summarized in this section demonstrates the importance of studying distributions at multiple levels of the hierarchical structure in bone and other tissues. We emphasize how characterization of collagen structure distributions by AFM and image analysis should inform research on disease mechanisms and treatments. Because collagen is so abundant in the body, greater scientific understanding of the relationship between changes in multiple levels of collagen hierarchical structure and observed physiological outcomes would streamline the development of new therapies for a wide variety of diseases. Research efforts should be focused on creating methods of accelerating molecular and fibril level analysis while ensuring sampling is representative of the heterogeneous tissue surface.

Distributions in Natural Nanoparticles. The previous two sections focused on characterizations of material distributions resulting from a laboratory synthesis, tissue biosynthesis, and tissue disease and drug treatment. Our more recent efforts combined aspects of this previous work on synthetic and natural materials: we investigated the relationship between distribution and function in intentionally created and controlled nanoparticles made of endogenous serum proteins. This research applied the analytical methods and statistical expertise our group developed through our earlier research described above. Specifically, we leveraged our experience making and characterizing dendrimer conjugates with precise ligand ratios and translated the AFM imaging and statistical methods developed in our collagen research to studying distributions in the protein nanoparticles. Our overarching goal was to understand the role serum folate binding protein (FBP) plays in folic acid (FA) and

DOI: 10.1021/acs.biomac.8b00375
Biomacromolecules 2018, 19, 1469–1484

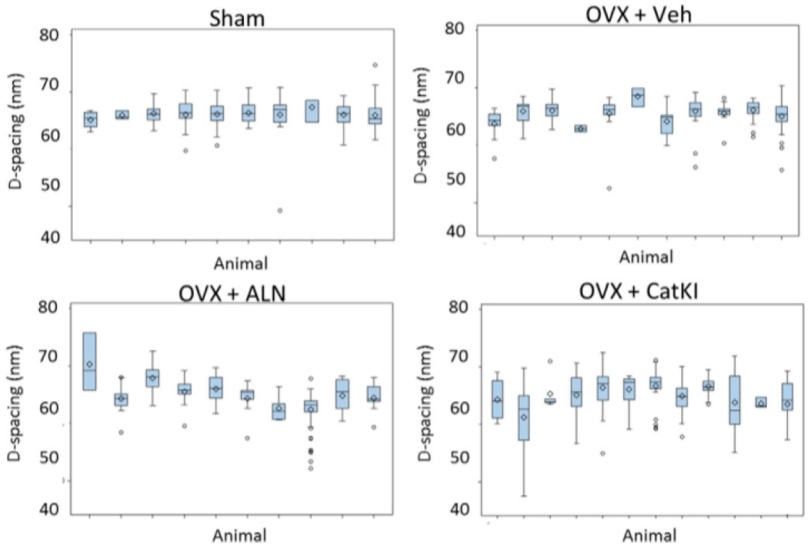

Figure 8. Boxplots of the *D*-spacing distribution of the collagen fibrils located in trabecular bundles obtained for sham, OVX+vehicle (VEH), OVX +ALN, and OVX+CatKI groups. There are significant differences in the degree of animal-to-animal variability across treatments in trabecular bone (p = 0.02, likelihood ratio Chi square test). The animal-to-animal variance for the OVX+VEH treatment was marginally significant (p = 0.074). Both drug treatments introduced significant animal-to-animal variability in the bundle *D*-spacing (p < 0.01). Reprinted from ref 21. Copyright 2016, with permission from the authors.

antifolate (aFA) drug trafficking. We also hypothesized that the protein itself could be used as a targeted vector, eliminating many of the challenges associated with stochastic or precisely defined conjugated polymers. Our conclusions highlight the need of a molecular approach to nanoparticle characterization in biological systems and the importance of employing complementary analytical methods.

Folate Binding Protein Nanoparticles (Highlighting Results from Refs 79 and 11). The structure and function of serum FBP have been extensively detailed by ourselves[11−13,51,79] and others.[80−95] For the purposes of this Perspective, it is important to note that FBP is derived from membrane-bound folate receptors (FRs) and plays a critical role in the complex, multiprotein process of cellular uptake of FA and in embryonic development.[92−102] FRs bind strongly to FA (nanomolar dissociation constant) and are overexpressed on many types of human cancers because rapidly dividing cancer cells require high levels of FA for DNA synthesis.[103−106] As a result, researchers, including ourselves as described in the ligand conjugation section above, have extensively explored FA as a targeting ligand.[6,11,22,27,51,101,102,107−113] Many of these conjugated targeted drug delivery agents suffer from the same heterogeneous distributions discussed above, but upon injection, they also interact with serum FBP before ever reaching the target cells. FA and the aFA drug methotrexate (MTX) have the same binding affinity for serum FBP as they do for FRs.[106] Additionally, the binding of FA or MTX to FBP triggers FBP aggregation and protein corona formation.[11−13,51] Protein coronas often define biological identity, so the trafficking, uptake, and therapeutic efficacy of these materials are dictated by FBP before they reach the targeted tumor cells.[114−120] FA-targeted therapies in vivo are likely to operate by different mechanisms than those predicted by in vitro experiments in the absence of soluble FBP, complicating interpretation of results and clinical translation.

Our first goal was to develop a better understanding of the interactions between FBP and small molecules (FA and aFAs). Earlier studies of serum FBP were limited by the detection limits of the bulk analytical techniques used, such as DLS, GPC, and IR spectroscopy.[80−88] Conversely, our attempts to use techniques like DLS were inhibited by the nanomolar protein concentrations required to reflect biological concentrations, the low scattering cross section of the nanoparticles, and biases toward detecting larger particle aggregates. Instead, we characterized FBP aggregation on a particle-by-particle basis using AFM (Figure 10).[11] This enabled investigation of FBP aggregation at physiologically and therapeutically relevant concentrations. In many ways, our approach was very similar to the fibril-by-fibril analysis with collagen, and many of the same image analysis techniques and statistical methods were used. The large number of particles imaged allowed for statistically robust analyses of the volume distributions. With hundreds to thousands of FBP nanoparticles (FBPNP) analyzed in each image, examining the distribution of particle volumes (as opposed to primarily relying on the mean volumes) proved critical in developing novel hypotheses on the biotrafficking of FA, MTX, and leucovorin (LEUC, a vitamer of FA).

We showed that, at physiological blood serum concentrations of FBP (2 nM), unligated FBP aggregates into nanoparticles comprised of ∼6−8 proteins. Interestingly, this agreed well with the reported 8-mer crystal structure of FR-α from which the majority of serum FBP is derived.[105] When FA was added to FBP at concentrations equivalent to FA deficiency in human adults, FBP aggregated into a bimodal distribution: nanoparticles of approximately 4 FBP and 600 FBP (Figure 10a). The nonuniform volume distribution of FBPNP at low FA concentrations is consistent with previously reported FA-induced apo-holo FBP aggregation.[82] The change in FBP volume distribution compared to healthy levels of FA suggests altered trafficking, biodistribution, and uptake processes that may be associated with symptoms of folate deficiency. Low concentrations of MTX resulted in larger nanoparticles (∼30 FBP), and low levels of LEUC completely inhibited aggregation (Figure 10b,c). When the concentration was increased to physiologically healthy or therapeutically relevant levels of FA, MTX, or LEUC, the FBPNP volume distribution became more

DOI: 10.1021/acs.biomac.8b00375
Biomacromolecules 2018, 19, 1469−1484

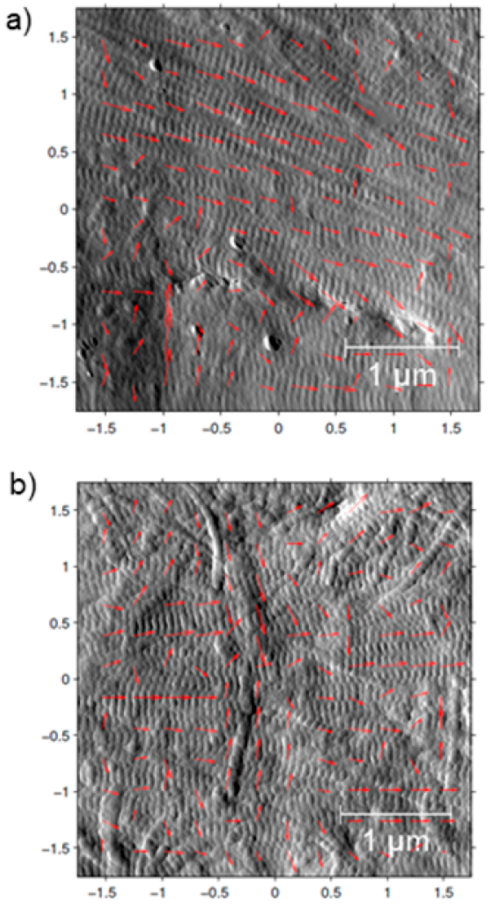

Figure 9. AFM images of collagen with arrows showing local alignment of collagen patches. The alignment was determined using an autocorrelation-based method. The arrow lengths are scaled to show the degree of alignment. (a) Collagen with a substantial concentration of parallel fibrils. (b) Collagen with a with a substantial concentration of oblique fibrils. Reprinted from ref 21. Copyright 2016, with permission from the authors.

monodisperse with 6−8 FBP per nanoparticle (Figure 10d−f), again the same as the number of proteins in the crystal structure.

Most surprisingly, our analyses of FBPNP volume distributions presented new hypotheses on the trafficking of LEUC and why it can be used as an FA rescue agent. Following treatment with MTX, LEUC is administered to mitigate toxicity caused by inhibition of FA activity. FA will not provide therapeutic benefit: LEUC must be used instead. The reason for this and the mechanism of action of LEUC has not been well understood. Most investigations of LEUC have focused at the cellular level, not considering the role of intravenous FBP.

Examination of the FBPNP volume distributions showed that FBPNP in the presence of high (therapeutic) doses of FBP was nearly identical to FBPNP containing therapeutic doses of MTX (Figure 11). The body would likely traffic both sets of FBPNP through the same biological pathways, preventing FA from acting as a rescue agent, especially because healthy concentrations of FA and therapeutic MTX are believed to enter cells via different uptake pathways,[121,122] potentially triggered by the FBP

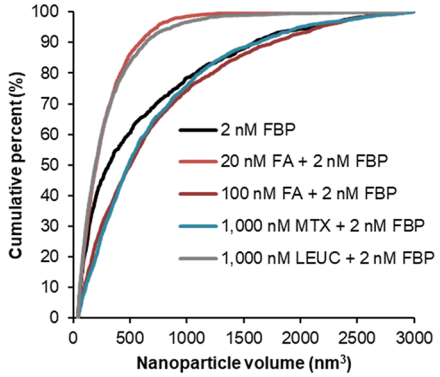

Figure 11. Cumulative density function (CDF) plots of selected measured volumes of FA-, MTX-, and LEUC-containing FBP nanoparticles. The similarity of the nanoparticle volume distributions was assessed using K−S statistics. The K−S testing showed the volume distributions of FBP nanoparticles formed from 20 nM FA + 2 nM FBP and 1000 nM LEUC + 2 nM FBP are not statistically different (p = 0.310). All other nanoparticle volume distributions were shown to be statistically different when evaluated with the K−S test. We hypothesize LEUC is effective as a folic acid rescue agent because the FBP nanoparticles formed at therapeutic concentrations of LEUC have the same volume distribution as the nanoparticles formed at healthy FA concentrations (20 nM). Adapted from ref 11 by permission of the Royal Society of Chemistry.

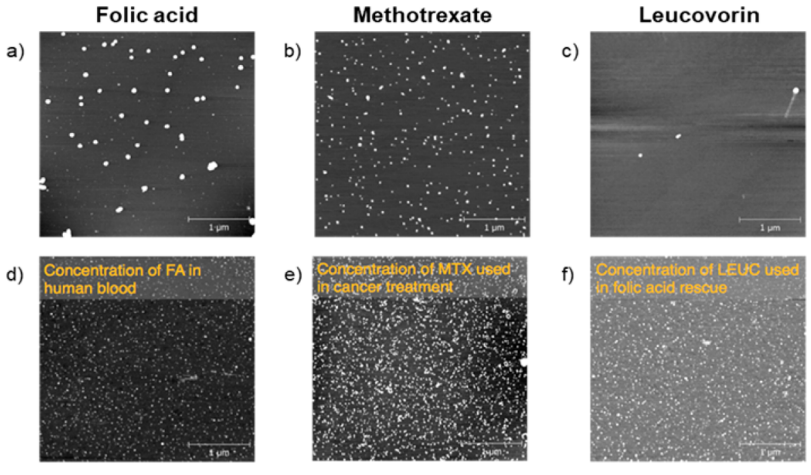

Figure 10. AFM images of FBP nanoparticles with folic acid, methotrexate, or leucovorin. (a−c) FBP and ligand present at 2 nM. (d) FA at 20 nM, FBP at 2 nM.(e) MTX at 1000 nM,; FBP at 2 nM. (f) LEUC at 1000 nM, FBP at 2 nM. Adapted from ref 11 by permission of the Royal Society of Chemistry.

DOI: 10.1021/acs.biomac.8b00375
Biomacromolecules 2018, 19, 1469−1484

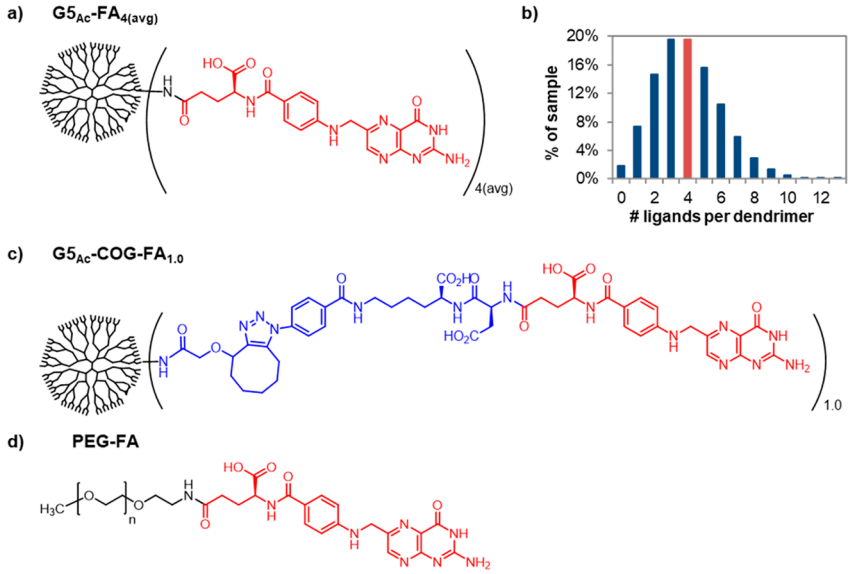

Figure 12. Representations of polymer-conjugate materials. For the PAMAM dendrimers, all terminal amines are acetylated following ligand conjugation. (a) Folic acid (FA, red) conjugated directly to G5 PAMAM (black), producing $G5_{Ac}$-$FA_{4(avg)}$; (b) distribution resulting from a stochastic conjugation with an average of four ligands and 93 arms; (c) FA (red) conjugated to G5 PAMAM (black) via a cyclooctyne glycolic acid (COG)-amino acid linker (blue), producing $G5_{Ac}$-COG-$FA_{1.0}$; (d) FA (red) conjugated to poly(ethylene glycol) (black). Reproduced with permission from ref 12. Copyright 2017, American Chemical Society.

aggregation state. Conversely, FBPNP with high doses of LEUC and physiological levels of FA had volume distributions that were not statistically different. This suggests LEUC is trafficked to cells through the same pathways as healthy levels of FA and can facilitate FA rescue by bypassing the MTX uptake pathway. These results provided the first hypothesis on the perplexing observation that FA itself cannot provide a therapeutic FA rescue benefit, requiring LEUC to be used instead. Had we only relied upon bulk measurements and mean size values in the data analysis, these connections likely would have been missed. The possible role of FBP particle size is particularly interesting in light of binary gate "lock and key" or "switch" analogies often employed when developing biological models of action. If particulate size is a factor in determining uptake rates, this suggests the analogy of a fuzzy logic gate is more appropriate for this case as opposed to a binary logic gate.

Conjugate-Dependent Interactions with Folate Binding Protein (Highlighting Results from Refs 51 and 12). Here, we bring this Perspective full circle to where we started with targeted polymer conjugates and illustrate how we applied lessons from all the research we have highlighted to this point. As we discussed above in detail, sample heterogeneity has plagued the translation into the clinic of FA-targeted polymer therapeutics.[2−10] Our particle-by-particle work on the interactions between small molecules (FA, MTX, and LEUC) with FBP[11,79] (as well as previous research with FA conjugates and FBP[6,11,22,27,51,112,113]) informed our guiding hypothesis that the identity of the conjugate itself could dictate the interaction with serum proteins. The combination of conjugation heterogeneity and unnatural serum protein aggregation processes likely leads to unexpected biological outcomes and failure in clinical translation efforts. The AFM and image analysis methods originally developed for our investigations of natural collagen distributions again proved critical in assessing FBP nanoparticle distributions. In contrast to our small molecule-FBP and collagen work, however, we used molecular level approaches in combination with solution fluorescence spectroscopy. The results discussed below demonstrate the risk in interpreting molecular interactions and structural information from only bulk techniques reporting averaged measurements. FBPNP distributions were dictated by both the chemical identity of the polymer scaffold and the conjugation method, but fluorescence spectroscopy experiments partially masked nuances in these results. The roles of both factors play in protein corona formation and in the ultimate fate of the targeted conjugate are often underappreciated.

Following a similar approach as we used on our studies of small molecule-FBP interactions, we directed our efforts toward characterizing the FA-conjugate-FBP interactions. We compared four FA-polymer conjugates: (1) $G5_{Ac}$-$FA_{4(avg)}$, (2) $G5_{Ac}$-COG-$FA_{1.0}$, and (3) poly(ethylene glycol)-FA (PEG-FA) of two different polymer chain lengths (Figure 12). The first, $G5_{Ac}$-$FA_{4(avg)}$, was a stochastic mixture with a mean of four FAs conjugated to the dendrimer (Figure 12a). On the basis of the Poisson distribution, ∼20% of the samples had four FA conjugated (Figure 12b). The second conjugate, $G5_{Ac}$-COG-$FA_{1.0}$, had precisely one FA conjugated through a cyclooctyne glycolic acid-amino acid linker (Figure 12c). This conjugate was synthesized and isolated via rp-HPLC methods similar to those described above.[6−9] The PEG-FA conjugates (Figure 12d) were commercially available. Chain lengths of 2 and 30 kDa were used in this study. NMR spectroscopy was used to quantify the concentration of active FA-conjugated material ($PEG_{2\ kDa}$-FA ∼ 25%; $PEG_{30\ kDa}$-FA ∼ 15%).

Tryptophan fluorescence quenching experiments, carried out in solution at protein concentrations an order of magnitude higher than physiological levels (58 nM vs 2 nM), indicated that free FA and $G5_{Ac}$-$FA_{4(avg)}$ induced similar changes in FBP conformation upon binding (Figure 13). This effect was observed whether the conjugate was added to an excess of FBP (Figure 13a) or FBP was added to an excess of FA (Figure 13b). The data also showed that any amount of FA (free or conjugated) was sufficient to induce conformational changes and subsequent fluorescence quenching throughout the entire protein population. $G5_{Ac}$-COG-$FA_{1.0}$ resulted in significantly larger protein

DOI: 10.1021/acs.biomac.8b00375
Biomacromolecules 2018, 19, 1469−1484

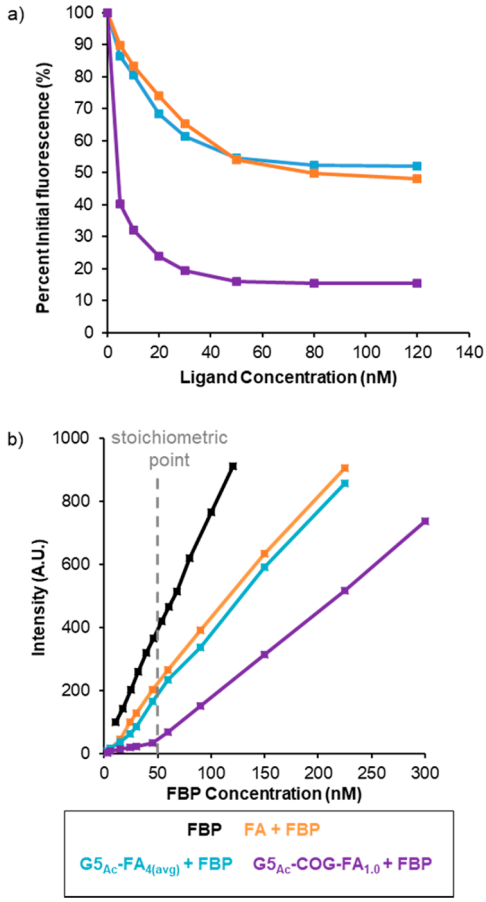

Figure 13. (a) Tryptophan fluorescence quenching upon addition of free FA or FA conjugated to FBP. FBP concentration was 58 nM. Note the strong fluorescence quenching at ~0.1 equiv of G5Ac-COG-$FA_{1.0}$. (b) Titration of FBP into FA (50 nM) and G5Ac-FA polymer conjugates (50 nM). FA materials produced conformational changes throughout the protein population. For both experiments, excitation = 280 nm, emission = 342 nm; pH 7.4 (1× PBS). Panel (b) reproduced with permission from ref 12. Copyright 2017, American Chemical Society.

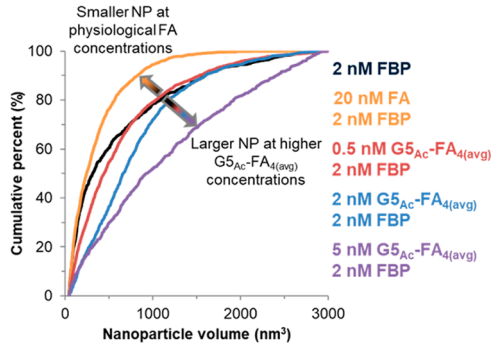

Figure 14. Cumulative density function (CDF) plots of the measured volume distributions of 2 nM FBP, 20 nM FA + 2 nM FBP, and G5Ac-$FA_{4(avg)}$ + FBP nanoparticles. The similarity of the nanoparticle volume distributions was assessed using K−S statistics, which showed all nanoparticle volume distributions to be statistically different. Analysis of the volume distributions indicated that FBP nanoparticle size increases with increasing G5Ac-$FA_{4(avg)}$ concentration. Reproduced with permission from ref 12. Copyright 2017, American Chemical Society.

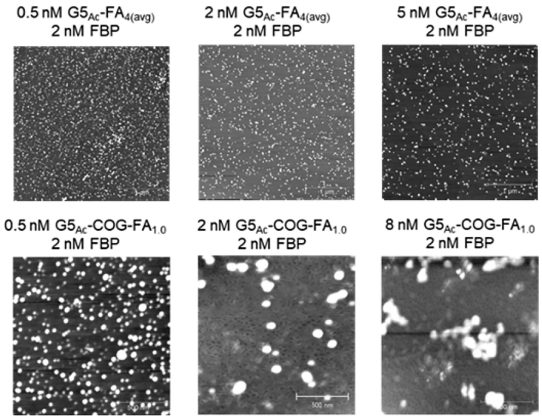

Figure 15. AFM images demonstrating the differences in aggregation when FBP is exposed to G5Ac-$FA_{4(avg)}$ and G5Ac-COG-$FA_{1.0}$. Reproduced with permission from ref 12. Copyright 2017 American Chemical Society.

conformational changes even in substoichiometric amounts of the conjugate. It bound essentially irreversibly to FBP and could not be displaced from the binding pocket by large excesses of free FA.[51] These data agreed with previous experiments demonstrating the same binding effect to surface-anchored FBP.[6] The PEG conjugates resulted in very little fluorescence quenching likely due to the long polymer chain blocking access to the binding pocket.[12,51]

Particle-by-particle analysis by AFM revealed important distinctions in the conjugate-protein interactions. The fluorescence data indicated free FA and G5Ac-$FA_{4(avg)}$ had similar binding interactions with FBPNP, but the FBPNP volume distributions were significantly different. FBPNP containing free FA were smaller than unligated FBPNP (Figure 14). Conversely, upon binding to G5Ac-$FA_{4(avg)}$, FBP rearranged into substantially larger nanoparticles. Consistent with the fluorescence data, G5Ac-COG-$FA_{1.0}$ resulted in very large aggregates with each conjugate inducing conformational changes and aggregation in more than one protein (Figure 15). This agrees well with our fluorescence data in Figure 13 demonstrating that, even with an excess of FBP, G5Ac-COG-$FA_{1.0}$ induced conformational changes throughout the protein population, resulting in fluorescence quenching. We postulate the long COG linker facilitates the strong binding interaction and FBP conformational changes, a phenomenon that we cover extensively elsewhere.[6,7,51] PEG conjugates of all chain lengths disrupted FBP aggregation, and no nanoparticles were observed.

In combination, these results illustrate both the risk of relying solely on bulk techniques to characterize these systems and the challenges of translating FA-targeted therapies into the clinic. The underlying assumption of FA-targeted therapies is that they are trafficked in the body like FA. That is, they should work because they go to cells and tissues with enhanced uptake of FA. The fluorescence spectroscopy data alone suggested that G5Ac-$FA_{4(avg)}$ would likely have been a good candidate for a targeted therapeutic because it induced the same degree of conformational change in FBP as induced by FA. However, as shown in Figure 14, the opposite trends in nanoparticle size upon ligand binding make it likely free FA and G5Ac-$FA_{4(avg)}$ would not follow the same trafficking and uptake pathways. Along the same lines, the very large aggregates with G5Ac-COG-$FA_{1.0}$ would be expected to exhibit different behavior in vivo. In contrast to the dendrimer conjugates, the AFM data showed no nanoparticles were present in samples containing PEG. The fluorescence spectroscopy data suggested a weaker binding interaction

DOI: 10.1021/acs.biomac.8b00375
Biomacromolecules 2018, 19, 1469−1484

between PEG-FA and FBP, but that alone does not demonstrate the extent of disruption in the system. PEG is the most common polymer in biomedical applications and is used to inhibit the formation of deleterious protein coronas on targeted conjugates.[118,123] It is therefore not surprising that PEG disrupted already existing FBPNP. PEG-containing FA-targeted conjugates likely would not follow the biotrafficking pathways of FA, and the inclusion of the polymer in rationally designed targeted vectors warrants consideration.

Implications for Targeted Drug Delivery. This Perspective has used PAMAM dendrimers as a case study for the challenges of both scaffold and conjugation heterogeneity associated with using polymers in targeted drug delivery. These issues do not just apply to PAMAM dendrimers but to all types of dendrimers and hyperbranched polymers (e.g., dendrons) used for biological applications.[49,50] This includes some of the most widely investigated scaffolds such as polyesters, poly(propyleneimines) (PPI), poly(2,2-bis(hydroxymethyl)propanoic acid (bis-MPA), and phosphorus-based dendrimers. All of these polymers have different advantages and disadvantages in terms of ease of synthesis and conjugation, solubility, and biocompatibility. In general, clinical translation of higher generation hyperbranched polymers of any type with multiple copies of different ligands will face the challenges associated with heterogeneity discussed above. In some cases, heterogeneity can be minimized through the synthesis process, and our group has previously reviewed the work in this area of making well-controlled polymers for biological applications.[10]

This is not to say that current dendrimers produced on large scales do not have potential as or in therapeutics. For example, Starpharma has received approval to market a dendritic therapy for bacterial vaginosis (VivaGel) and is testing the material for a number of other sexual health-related applications.[124] Although this clinical success of a dendritic therapy is noteworthy, VivaGel differs from the PAMAM dendrimers discussed here in several important ways. VivaGel is a generation 3 (G3) poly(lysine) dendrimer with 32 surface groups. Because fewer synthetic steps are required to make G3 poly(lysine) dendrimers compared to commonly used G5 PAMAM dendrimers, VivaGel has a lower incidence of defects in the scaffold. This produces a material with less heterogeneity and that is more, but not entirely, molecular. Furthermore, the surface naphthyl disulfonate groups are incorporated as part of the synthesis of the dendrimer, reducing heterogeneity resulting from conjugation. VivaGel is also administered differently than the targeted dendrimer systems discussed above: it is applied as a gel or incorporated into personal lubricants. VivaGel is not injected or ingested, and it is not targeted; it therefore avoids complications associated with opsonization and off-target uptake. Highlighting these differences between VivaGel and other types of dendrimer therapeutics is not intended to detract from the success of this product but rather to illustrate why VivaGel has had comparatively smooth translation into the clinic.

Starpharma has been making efforts to use its poly(lysine) dendrimer technology in targeted cancer therapeutics. The company is carrying out Phase II clinical trials with PEGylated poly(lysine) dendrimers conjugated to docetaxel (DEP-docetaxel). Conjugating not one but two species to the dendrimer scaffold has introduced a significant amount of heterogeneity into the system, as discussed in detail above, and the full physiological implications of this heterogeneity are likely not known. Like with many other targeted polymer therapies that have been tested in clinical trials, DEP-docetaxel produces promising results in vitro and in vivo in small animal models. However, the translation to treatment in humans is often difficult. When tested in humans, the majority of targeted polymer therapeutics do not produce the same therapeutic benefits or reduce adverse side effects. It will be highly significant if DEP-docetaxel (and related systems from Starpharma) avoids these translational challenges. The results could provide valuable insights for the research community into expediting clinical translation of targeted polymer therapeutics.

The drug delivery research community should also give consideration to moving toward systems that do not suffer from the challenges of scaffold and conjugation heterogeneity. Some researchers have started to use serum protein-based vectors, which not only address issues of heterogeneity but also the problems of opsonization, immunogenicity, and biodegradability associated with synthetic drug delivery vectors. One of the most powerful achievements in drug delivery over the past decade is Abraxane, an albumin-bound form of paclitaxel.[125−129] Researchers recently reported a cancer vaccine using albumin as a carrier showing great promise in in vivo trials.[130] Many more albumin-based approaches are currently in clinical trials. Taking advantage of natural protein aggregation processes may indeed provide a key to avoiding the challenges of heterogeneous distributions in synthetic and natural drug delivery materials.

One of the notable aspects of these recent successes with protein-based vectors is that protein aggregation is often considered to be an indication of disease or dysfunction, such as β-amyloid formation associated with Alzheimer's disease.[131] However, decade's worth of FBP aggregation data, including ours, indicate that FBP aggregation is a healthy and natural process and that understanding the changes in particle aggregate distribution as a function of changes in conditions is critical to understanding and controlling function.[11,80−88] FBP plays a central role in cellular uptake of FA and is essential for healthy embryonic development. In our own research, we are currently investigating the possibility of leveraging the action of FBP for drug delivery applications.

CONCLUSIONS AND FUTURE PERSPECTIVES

In this Perspective, we examined almost two decades of our research team's work to characterize heterogeneous distributions in multivalent polymers, collagen hierarchical structure, and serum protein nanoparticles. By tracing through the history of our work, we illustrated how our most recent work on protein nanoparticles leveraged all our collaborative knowledge and expertise on distributions. We showed how our methods were widely applicable and translated between research projects characterizing distributions created in both synthetic materials and inherently present in natural tissues. In each of the research cases, we emphasized how our unique molecular level analytical and statistical approaches were critical for interpreting data, understanding biological results, and facilitating development of new insights and hypotheses that would be missed through bulk measurements. As a set, the examples and discussion included here are intended to make a convincing case for the importance of a molecular level view of biological materials. We encourage investment in the development of methods to expand scientific understanding of the interplay between molecular level distributions and structural variation and function.

Relatively new techniques are starting to bridge the gap between bulk analytical methods and molecular level analysis. For example, combined AFM and IR spectroscopy allows for IR spectra to be acquired with as high as ~10 nm lateral resolution

DOI: 10.1021/acs.biomac.8b00375
Biomacromolecules 2018, 19, 1469−1484

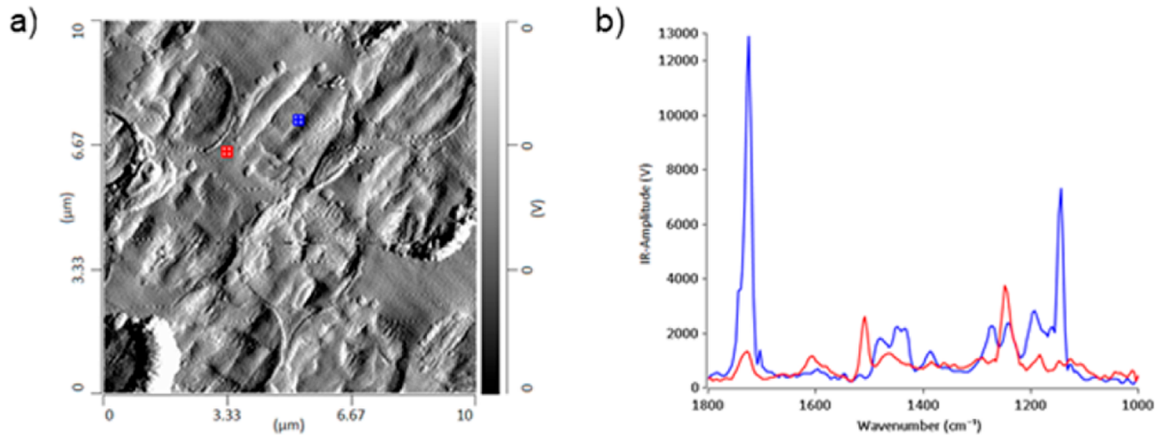

Figure 16. Example of AFM-IR with (a) a deflection image and (b) IR spectra acquired at locations indicated by the squares on the image. The blue spectrum clearly shows the signals from poly(methyl methacrylate) beads (the circles) as compared to the epoxy (red trace). Acquired on a nanoIR2 from Anasys Instruments.

(Figure 16). In our current research efforts, we are employing AFM-IR to examine changes in mineral-collagen ratio throughout bone as a function of disease and treatment, identify microdamage that leads to failure in anterior cruciate ligaments, investigate uptake of nanoplastics into mussels, study the chemical composition of atmospheric particles, and characterize the composition of a variety of composite polymers. As techniques that enable nanoscale, molecular, or chemical identity level characterization (e.g., AFM-IR, AFM-mass spectrometry, and single particle tracking) become more widely available, the broader research community will have more capacity to address the challenges of heterogeneity and distributions presented here.

AUTHOR INFORMATION

Corresponding Author

*E-mail: mark.banaszakholl@monash.edu.

ORCID

Rachel L. Merzel: 0000-0002-0637-3970

Mark M. Banaszak Holl: 0000-0001-7759-7456

Notes

The authors declare no competing financial interest.

ACKNOWLEDGMENTS

M.M.B.H. and B.G.O. acknowledge the The National Cancer Institute (RO1 CA119409), the National Institute of Biomedical Imaging and Bioengineering (RO1 EB005028), an IISP grant from Merck Inc., the Burroughs Welcome Fund, and the National Science Foundation (CMMI 1634680) for generous support of the research program described in this review. R.L.M. acknowledges a National Science Foundation Graduate Research Fellowship under Grant No. DGE 1256260. Two decades of important medical collaborations with James R. Baker, Jr. M.D., Clifford Les, DVM, Ph.D., Brent B. Ward M.D., D.D.S., and Edward M. Wojtys, M.D. are gratefully acknowledged. We are also greatly indebted to our statistical collaborators Edward D. Rothman and Kathleen B. Welch.

REFERENCES

(1) Chen, J.; Ahn, T.; Colón-Bernal, I. D.; Kim, J.; Banaszak Holl, M. M. The Relationship of Collagen Structural and Compositional Heterogeneity to Tissue Mechanical Properties: A Chemical Perspective. *ACS Nano* **2017**, *11*, 10665−10671.

(2) Mullen, D. G.; Fang, M.; Desai, A.; Baker, J. R.; Orr, B. G.; Banaszak Holl, M. M. A Quantitative Assessment of Nanoparticle−Ligand Distributions: Implications for Targeted Drug and Imaging Delivery in Dendrimer Conjugates. *ACS Nano* **2010**, *4*, 657−670.

(3) Mullen, D. G.; Banaszak Holl, M. M. Heterogeneous Ligand−Nanoparticle Distributions: A Major Obstacle to Scientific Understanding and Commercial Translation. *Acc. Chem. Res.* **2011**, *44*, 1135−1145.

(4) van Dongen, M. A.; Desai, A.; Orr, B. G.; Baker, J. R.; Banaszak Holl, M. M. Banaszak Holl, M. M. Quantitative Analysis of Generation and Branch Defects in G5 Poly(amidoamine) Dendrimer. *Polymer* **2013**, *54*, 4126−4133.

(5) Mullen, D. G.; Desai, A.; van Dongen, M. A.; Barash, M.; Baker, J. R.; Banaszak Holl, M. M. Best Practices for Purification and Characterization of PAMAM. *Macromolecules* **2012**, *45*, 5316−5320.

(6) van Dongen, M. A.; Silpe, J. E.; Dougherty, C. A.; Kanduluru, A. K.; Choi, S. K.; Orr, B. G.; Low, P. S.; Banaszak Holl, M. M. Avidity Mechanism of Dendrimer−Folic Acid Conjugates. *Mol. Pharmaceutics* **2014**, *11*, 1696−1706.

(7) van Dongen, M. A.; Rattan, R.; Silpe, J.; Dougherty, C.; Michmerhuizen, N. L.; Van Winkle, M.; Huang, B.; Choi, S. K.; Sinniah, K.; Orr, B. G.; et al. Poly(amidoamine) Dendrimer−Methotrexate Conjugates: The Mechanism of Interaction with Folate Binding Protein. *Mol. Pharmaceutics* **2014**, *11*, 4049−4058.

(8) Dougherty, C. A.; Furgal, J. C.; van Dongen, M. A.; Goodson, T.; Banaszak Holl, M. M.; Manono, J.; DiMaggio, S. Isolation and Characterization of Precise Dye/Dendrimer Ratios. *Chem. - Eur. J.* **2014**, *20*, 4638−4645.

(9) Dougherty, C. A.; Vaidyanathan, S.; Orr, B. G.; Banaszak Holl, M. M. Fluorophore:Dendrimer Ratio Impacts Cellular Uptake and Intracellular Fluorescence Lifetime. *Bioconjugate Chem.* **2015**, *26*, 304−315.

(10) van Dongen, M. A.; Dougherty, C. A.; Banaszak Holl, M. M. . Multivalent Polymers for Drug Delivery and Imaging: The Challenges of Conjugation. *Biomacromolecules* **2014**, *15*, 3215−3234.

(11) Merzel, R. L.; Boutom, S. M.; Chen, J.; Frey, C.; Shedden, K.; Marsh, E. N. G.; Banaszak Holl, M. M. Folate Binding Protein: Therapeutic Natural Nanotechnology for Folic Acid, Methotrexate, and Leucovorin. *Nanoscale* **2017**, *9*, 2603−2615.

(12) Merzel, R. L.; Frey, C.; Chen, J.; Garn, R.; Van Dongen, M.; Dougherty, C. A.; Kandaluru, A. K.; Low, P. S.; Marsh, E. N. G.; Banaszak Holl, M. M. Conjugation Dependent Interaction of Folic Acid with Folate Binding Protein. *Bioconjugate Chem.* **2017**, *28*, 2350−2360.

(13) Chen, J.; Klem, S.; Jones, A. K.; Orr, B.; Banaszak Holl, M. M. Folate-Binding Protein Self-Aggregation Drives Agglomeration of Folic Acid Targeted Iron Oxide Nanoparticles. *Bioconjugate Chem.* **2017**, *28*, 81−87.

DOI: 10.1021/acs.biomac.8b00375
Biomacromolecules 2018, 19, 1469−1484

(14) Erickson, B.; Fang, M.; Wallace, J. M.; Orr, B. G.; Les, C. M.; Banaszak Holl, M. M. Nanoscale Structure of Type I Collagen Fibrils: Quantitative Measurement of D-Spacing. *Biotechnol. J.* **2013**, *8*, 117−126.
(15) Wallace, J. M.; Chen, Q.; Fang, M.; Erickson, B.; Orr, B. G.; Banaszak Holl, M. M. Type I Collagen Exists as a Distribution of Nanoscale Morphologies in Teeth, Bones, and Tendons. *Langmuir* **2010**, *26*, 7349−7354.
(16) Wallace, J. M.; Erickson, B.; Les, C. M.; Orr, B. G.; Banaszak Holl, M. M. Distribution of Type I Collagen Morphologies in Bone: Relation to Estrogen Depletion. *Bone* **2010**, *46*, 1349−1354.
(17) Fang, M.; Liroff, K. G.; Turner, A. S.; Les, C. M.; Orr, B. G.; Banaszak Holl, M. M. B. Estrogen Depletion Results in Nanoscale Morphology Changes in Dermal Collagen. *J. Invest. Dermatol.* **2012**, *132*, 1791−1797.
(18) Fang, M.; Goldstein, E. L.; Turner, A. S.; Les, C. M.; Orr, B. G.; Fisher, G. J.; Welch, K. B.; Rothman, E. D.; Banaszak Holl, M. M. Type I Collagen D-Spacing in Fibril Bundles of Dermis, Tendon, and Bone: Bridging between Nano- and Micro-Level Tissue Hierarchy. *ACS Nano* **2012**, *6*, 9503−9514.
(19) Fang, M.; Holl, M. M. B. Variation in Type I Collagen Fibril Nanomorphology: The Significance and Origin. *BoneKEy Rep.* **2013**, *2*, 1.
(20) Cauble, M. A.; Rothman, E.; Welch, K.; Fang, M.; Duong, L. T.; Pennypacker, B. L.; Orr, B. G.; Banaszak-Holl, M. M. Alteration of Type I Collagen Microstructure Induced by Estrogen Depletion Can Be Prevented with Drug Treatment. *BoneKEy Rep.* **2015**, *4*, 697.
(21) Cauble, M. A.; Muckley, M. J.; Fang, M.; Fessler, J. A.; Welch, K.; Rothman, E. D.; Orr, B. G.; Duong, L. T.; Holl, M. M. B. Estrogen Depletion and Drug Treatment Alter the Microstructure of Type I Collagen in Bone. *Bone Reports* **2016**, *5*, 243−251.
(22) Mullen, D. G.; McNerny, D. Q.; Desai, A.; Cheng, X.; DiMaggio, S. C.; Kotlyar, A.; Zhong, Y.; Qin, S.; Kelly, C. V.; Thomas, T. P.; et al. Design, Synthesis, and Biological Functionality of a Dendrimer-Based Modular Drug Delivery Platform. *Bioconjugate Chem.* **2011**, *22*, 679−689.
(23) Landmark, K. J.; DiMaggio, S.; Ward, J.; Kelly, C.; Vogt, S.; Hong, S.; Kotlyar, A.; Myc, A.; Thomas, T. P.; Penner-Hahn, J. E.; et al. Synthesis, Characterization, and in Vitro Testing of Superparamagnetic Iron Oxide Nanoparticles Targeted Using Folic Acid-Conjugated Dendrimers. *ACS Nano* **2008**, *2*, 773−783.
(24) Majoros, I. J.; Myc, A.; Thomas, T.; Mehta, C. B.; Baker, J. R. PAMAM Dendrimer-Based Multifunctional Conjugate for Cancer Therapy: Synthesis, Characterization, and Functionality. *Biomacromolecules* **2006**, *7*, 572−579.
(25) Li, M.-H.; Choi, S. K.; Thomas, T. P.; Desai, A.; Lee, K.-H.; Kotlyar, A.; Banaszak Holl, M. M.; Baker, J. R., Jr Dendrimer-Based Multivalent Methotrexates as Dual Acting Nanoconjugates for Cancer Cell Targeting. *Eur. J. Med. Chem.* **2012**, *47*, 560−572.
(26) Baker, J. R. Why I Believe Nanoparticles Are Crucial as a Carrier for Targeted Drug Delivery. *WIREs. Nanomed. Nanobiotechnol.* **2013**, *5*, 423−429.
(27) Ward, B. B.; Dunham, T.; Majoros, I. J.; Baker, J. R. Targeted Dendrimer Chemotherapy in an Animal Model for Head and Neck Squamous Cell Carcinoma. *J. Oral Maxillofac. Surg.* **2011**, *69*, 2452−2459.
(28) Quintana, A.; Raczka, E.; Piehler, L.; Lee, I.; Myc, A.; Majoros, I.; Patri, A. K.; Thomas, T.; Mulé, J.; Baker, J. R., Jr. Design and Function of a Dendrimer-Based Therapeutic Nanodevice Targeted to Tumor Cells through the Folate Receptor. *Pharm. Res.* **2002**, *19*, 1310−1316.
(29) Majoros, I. J.; Thomas, T. P.; Mehta, C. B.; Baker, J. R. Poly(amidoamine) Dendrimer-Based Multifunctional Engineered Nanodevice for Cancer Therapy. *J. Med. Chem.* **2005**, *48*, 5892−5899.
(30) Kukowska-Latallo, J. F.; Candido, K. A.; Cao, Z.; Nigavekar, S. S.; Majoros, I. J.; Thomas, T. P.; Balogh, L. P.; Khan, M. K.; Baker, J. R. Nanoparticle Targeting of Anticancer Drug Improves Therapeutic Response in Animal Model of Human Epithelial Cancer. *Cancer Res.* **2005**, *65*, 5317.
(31) Betley, T. A.; Hessler, J. A.; Mecke, A.; Banaszak Holl, M. M.; Orr, B. G.; Uppuluri, S.; Tomalia, D. A.; Baker, J. R. Tapping Mode Atomic Force Microscopy Investigation of Poly(amidoamine) Core−Shell Tecto(dendrimers) Using Carbon Nanoprobes. *Langmuir* **2002**, *18*, 3127−3133.
(32) Betley, T. A.; Banaszak Holl, M. M.; Orr, B. G.; Swanson, D. R.; Tomalia, D. A.; Baker, J. R. Tapping Mode Atomic Force Microscopy Investigation of Poly(amidoamine) Dendrimers: Effects of Substrate and pH on Dendrimer Deformation. *Langmuir* **2001**, *17*, 2768−2773.
(33) Baker, J. R.; Quintana, A.; Piehler, L.; Banazak-Holl, M.; Tomalia, D.; Raczka, E. The Synthesis and Testing of Anti-Cancer Therapeutic Nanodevices. Biomed. *Biomed. Microdevices* **2001**, *3*, 61−69.
(34) Hong, S.; Bielinska, A. U.; Mecke, A.; Keszler, B.; Beals, J. L.; Shi, X.; Balogh, L.; Orr, B. G.; Baker, J. R.; Banaszak Holl, M. M. Interaction of Poly(amidoamine) Dendrimers with Supported Lipid Bilayers and Cells: Hole Formation and the Relation to Transport. *Bioconjugate Chem.* **2004**, *15*, 774−782.
(35) Peer, D.; Karp, J. M.; Hong, S.; Farokhzad, O. C.; Margalit, R.; Langer, R. Nanocarriers as an Emerging Platform for Cancer Therapy. *Nat. Nanotechnol.* **2007**, *2*, 751−760.
(36) Fang, J.; Nakamura, H.; Maeda, H. The EPR Effect: Unique Features of Tumor Blood Vessels for Drug Delivery, Factors Involved, and Limitations and Augmentation of the Effect. *Adv. Drug Delivery Rev.* **2011**, *63*, 136−151.
(37) Greish, K. Enhanced Permeability and Retention (EPR) Effect for Anticancer Nanomedicine Drug Targeting. In *Cancer Nanotechnology*; Grobmyer, S. R., Moudgil, B. M., Eds.; Humana Press, 2010; Vol. *624*, pp 25−37.
(38) Pasut, G.; Veronese, F. M. Polymer-Drug Conjugation, Recent Achievements and General Strategies. *Progress in Polymer Science (Oxford)*; Pergamon, August 1, 2007; pp 933−961.
(39) Duncan, R.; Gaspar, R. Nanomedicine(s) under the Microscope. *Mol. Pharmaceutics* **2011**, *8*, 2101−2141.
(40) Duncan, R.; Richardson, S. C. W. Endocytosis and Intracellular Trafficking as Gateways for Nanomedicine Delivery: Opportunities and Challenges. *Mol. Pharmaceutics* **2012**, *9*, 2380−2402.
(41) Svenson, S. Theranostics: Are We There Yet? *Molecular Pharmaceutics*; American Chemical Society, March 4, 2013; pp 848−856.
(42) van der Meel, R.; Vehmeijer, L. J. C.; Kok, R. J.; Storm, G.; van Gaal, E. V. B. Ligand-Targeted Particulate Nanomedicines Undergoing Clinical Evaluation: Current Status. *Adv. Drug Delivery Rev.* **2013**, *65*, 1284−1298.
(43) Röglin, L.; Lempens, E. H. M.; Meijer, E. W. A Synthetic "tour de Force": Well-Defined Multivalent and Multimodal Dendritic Structures for Biomedical Applications. Angewandte Chemie - International Edition. *Angew. Chem., Int. Ed.* **2011**, *50*, 102−112.
(44) Kelkar, S. S.; Reineke, T. M. Theranostics: Combining Imaging and Therapy. *Bioconjugate Chem.* **2011**, *22*, 1879−1903.
(45) Lee, C. C.; MacKay, J. A.; Fréchet, J. M. J. J.; Szoka, F. C. Designing Dendrimers for Biological Applications. *Nat. Biotechnol.* **2005**, *23*, 1517−1526.
(46) Boas, U.; Heegaard, P. M. H. Dendrimers in Drug Research. *Chem. Soc. Rev.* **2004**, *33*, 43.
(47) Temming, K.; Schiffelers, R. M.; Molema, G.; Kok, R. J. RGD-Based Strategies for Selective Delivery of Therapeutics and Imaging Agents to the Tumour Vasculature. *Drug Resist. Updates* **2005**, *8*, 381−402.
(48) Haag, R.; Kratz, F. Polymer Therapeutics: Concepts and Applications. *Angew. Chem., Int. Ed.* **2006**, *45*, 1198−1215.
(49) Kannan, R. M.; Nance, E.; Kannan, S.; Tomalia, D. A. Emerging Concepts in Dendrimer-Based Nanomedicine: From Design Principles to Clinical Applications. *J. Intern. Med.* **2014**, *276*, 579−617.
(50) Mignani, S.; Rodrigues, J.; Tomas, H.; Zablocka, M.; Shi, X.; Caminade, A.-M.; Majoral, J.-P. Dendrimers in Combination with Natural Products and Analogues as Anti-Cancer Agents. *Chem. Soc. Rev.* **2018**, *47*, 514−532.
(51) Chen, J.; van Dongen, M. A.; Merzel, R. L.; Dougherty, C. A.; Orr, B. G.; Kanduluru, A. K.; Low, P. S.; Marsh, E. N. G.; Banaszak Holl, M.

DOI: 10.1021/acs.biomac.8b00375
Biomacromolecules 2018, 19, 1469−1484

M. Substrate-Triggered Exosite Binding: Synergistic Dendrimer/Folic Acid Action for Achieving Specific, Tight-Binding to Folate Binding Protein. *Biomacromolecules* **2016**, *17*, 922−927.
(52) Hakem, I. F.; Leech, A. M.; Johnson, J. D.; Donahue, S. J.; Walker, J. P.; Bockstaller, M. R. Understanding Ligand Distributions in Modified Particle and Particlelike Systems. *J. Am. Chem. Soc.* **2010**, *132*, 16593−16598.
(53) Hakem, I. F.; Leech, A. M.; Bohn, J.; Walker, J. P.; Bockstaller, M. R. Analysis of Heterogeneity in Nonspecific PEGylation Reactions of Biomolecules. *Biopolymers* **2013**, *99*, 427−435.
(54) Larson, N.; Ghandehari, H. *Polymeric Conjugates for Drug Delivery. Chemistry of Materials*; American Chemical Society, March 13, 2012; pp 840−853.
(55) Mintzer, M. A.; Simanek, E. E. *Nonviral Vectors for Gene Delivery. Chemical Reviews*; American Chemical Society, February 11, 2009; pp 259−302.
(56) Mintzer, M. A.; Grinstaff, M. W. Biomedical Applications of Dendrimers: A Tutorial. *Chem. Soc. Rev.* **2011**, *40*, 173−190.
(57) Chen, M.; Yin, M. Design and Development of Fluorescent Nanostructures for Bioimaging; *Progress in Polymer Science*; Pergamon, February 1, 2014; pp 365−395.
(58) Pansare, V. J.; Hejazi, S.; Faenza, W. J.; Prud'homme, R. K. Review of Long-Wavelength Optical and NIR Imaging Materials: Contrast Agents, Fluorophores, and Multifunctional Nano Carriers. *Chem. Mater.* **2012**, *24*, 812−827.
(59) He, C.; Hu, Y.; Yin, L.; Tang, C.; Yin, C. Effects of Particle Size and Surface Charge on Cellular Uptake and Biodistribution of Polymeric Nanoparticles. *Biomaterials* **2010**, *31*, 3657−3666.
(60) Philipp Seib, F.; Jones, A. T.; Duncan, R. Establishment of Subcellular Fractionation Techniques to Monitor the Intracellular Fate of Polymer Therapeutics I. Differential Centrifugation Fractionation B16F10 Cells and Use to Study the Intracellular Fate of HPMA Copolymer−doxorubicin. *J. Drug Target.* **2006**, *14*, 375−390.
(61) Yang, Y.; Sunoqrot, S.; Stowell, C.; Ji, J.; Lee, C.-W.; Kim, J. W.; Khan, S. A.; Hong, S. Effect of Size, Surface Charge, and Hydrophobicity of Poly(amidoamine) Dendrimers on Their Skin Penetration. *Biomacromolecules* **2012**, *13*, 2154−2162.
(62) Chen, L. C.; Lloyd, W. R.; Chang, C. W.; Sud, D.; Mycek, M. A. Fluorescence Lifetime Imaging Microscopy for Quantitative Biological Imaging. *Methods Cell Biol.* **2013**, *114*, 457−488.
(63) Ottani, V.; Martini, D.; Franchi, M.; Ruggeri, A.; Raspanti, M. Hierarchical Structures in Fibrillar Collagens. *Micron* **2002**, *33*, 587−596.
(64) Kadler, K. E.; Baldock, C.; Bella, J.; Boot-Handford, R. P. *J. Cell Sci.* **2007**, *120*, 1955−1958.
(65) Kadler, K. E.; Holmes, D. F.; Trotter, J. A.; Chapman, J. A. Collagen Fibril Formation. *Biochem. J.* **1996**, *316*, 1−11.
(66) Hulmes, D. J. S. Building Collagen Molecules, Fibrils, and Suprafibrillar Structures. *J. Struct. Biol.* **2002**, *137*, 2−10.
(67) Li, T.; Chang, S. W.; Rodriguez-Florez, N.; Buehler, M. J.; Shefelbine, S.; Dao, M.; Zeng, K. Studies of Chain Substitution Caused Sub-Fibril Level Differences in Stiffness and Ultrastructure of Wildtype and Oim/oim Collagen Fibers Using Multifrequency-AFM and Molecular Modeling. *Biomaterials* **2016**, *107*, 15−22.
(68) Hodge, A. J.; Petruska, J. A. *Recent Studies with the Electron Microscope on Ordered Aggregates of the Tropocollagen Molecule*; Academic Press: New York, 1963.
(69) Orgel, J. P. R. O.; Irving, T. C.; Miller, A.; Wess, T. J. Microfibrillar Structure of Type I Collagen in Situ. *Proc. Natl. Acad. Sci. U. S. A.* **2006**, *103*, 9001−9005.
(70) Miller, A.; Wray, J. S. Molecular Packing in Collagen. *Nature* **1971**, *230*, 437−439.
(71) Hulmes, D. J. S.; Miller, A. Quasi-Hexagonal Molecular Packing in Collagen Fibrils [34]. *Nature* **1979**, *282*, 878−880.
(72) Fraser, R. D. B.; MacRae, T. P.; Miller, A.; Suzuki, E. Molecular Conformation and Packing in Collagen Fibrils. *J. Mol. Biol.* **1983**, *167*, 497−521.
(73) Fraser, R. D. B.; MacRae, T. P.; Miller, A. Molecular Packing in Type I Collagen Fibrils. *J. Mol. Biol.* **1987**, *193*, 115−125.
(74) Trus, B. L.; Piez, K. A. Compressed Microfibril Models of the Native Collagen Fibril. *Nature* **1980**, *286*, 300−301.
(75) Traub, W.; Piez, K. A. The Chemistry and Structure of Collagen. *Adv. Protein Chem.* **1971**, *25*, 243−352.
(76) Piez, K. A.; Trus, B. L. A New Model for Packing of Type-I Collagen Molecules in the Native Fibril. *Biosci. Rep.* **1981**, *1*, 801−810.
(77) Brodsky, B.; Eikenberry, E. F. [5] Characterization of Fibrous Forms of Collagen. *Methods Enzymol.* **1982**, *82*, 127−174.
(78) Hulmes, D. J.; Wess, T. J.; Prockop, D. J.; Fratzl, P. Radial Packing, Order, and Disorder in Collagen Fibrils. *Biophys. J.* **1995**, *68*, 1661−1670.
(79) Merzel, R. L.; Chen, J.-J.; Marsh, E. N. G.; Holl, M. M. B. Folate Binding protein—Outlook for Drug Delivery Applications. *Chin. Chem. Lett.* **2015**, *26*, 426−430.
(80) Pedersen, T.; Svendsen, I.; Hansen, S.; Holm, J.; Lyngbye, J. Aggregation of a Folate-Binding Protein from Cow's Milk. *Carlsberg Res. Commun.* **1980**, *45*, 161−166.
(81) Hansen, S. I.; Holm, J.; Lyngbye, J.; Pedersen, T. G.; Svendsen, I. Dependence of Aggregation and Ligand Affinity on the Concentration of the Folate-Binding Protein from Cow's Milk. *Arch. Biochem. Biophys.* **1983**, *226*, 636−642.
(82) Holm, J.; Schou, C.; Babol, L. N.; Lawaetz, A. J.; Bruun, S. W.; Hansen, M. Z.; Hansen, S. I. The Interrelationship between Ligand Binding and Self-Association of the Folate Binding Protein. The Role of Detergent?tryptophan Interaction. *Biochim. Biophys. Acta, Gen. Subj.* **2011**, *1810*, 1330−1339.
(83) Holm, J.; Lawaetz, A. J.; Hansen, S. I. Ligand Binding Induces a Sharp Decrease in Hydrophobicity of Folate Binding Protein Assessed by 1-Anilinonaphthalene-8-Sulphonate Which Suppresses Self-Association of the Hydrophobic Apo-Protein. *Biochem. Biophys. Res. Commun.* **2012**, *425*, 19−24.
(84) Christensen, U.; Holm, J.; Hansen, S. I. Stopped-Flow Kinetic Studies of the Interaction of Bovine Folate Binding Protein (FBP) and Folate. *Biosci. Rep.* **2006**, *26*, 291−299.
(85) Kaarsholm, N. C.; Kolstrup, A.-M.; Danielsen, S. E.; Holm, J.; Hansen, S. I. Ligand-Induced Conformation Change in Folate-Binding Protein. *Biochem. J.* **1993**, *292*, 921−925.
(86) Holm, J.; Babol, L. N.; Markova, N.; Lawaetz, A. J.; Hansen, S. I. The Interrelationship between Ligand Binding and Thermal Unfolding of the Folate Binding Protein. The Role of Self-Association and pH. *Biochim. Biophys. Acta, Proteins Proteomics* **2014**, *1844*, 512−519.
(87) Bruun, S. W.; Holm, J.; Hansen, S. I.; Jacobsen, S. Application of Near-Infrared and Fourier Transform Infrared Spectroscopy in the Characterization of Ligand-Induced Conformation Changes in Folate Binding Protein Purified from Bovine Milk: Influence of Buffer Type and pH. *Appl. Spectrosc.* **2006**, *60*, 737−746.
(88) Bruun, S. W.; Holm, J.; Hansen, S. I.; Andersen, C. M.; Norgaard, L.; Nørgaard, L. A Chemometric Analysis of Ligand-Induced Changes in Intrinsic Fluorescence of Folate Binding Protein Indicates a Link between Altered Conformational Structure and Physico-Chemical Characteristics. *Appl. Spectrosc.* **2009**, *63*, 1315−1322.
(89) Kur, E.; Mecklenburg, N.; Cabrera, R. M.; Willnow, T. E.; Hammes, A. LRP2Mediates Folate Uptake in the Developing Neural Tube. *J. Cell Sci.* **2014**, *127*, 2261−2268.
(90) Birn, H.; Zhai, X. Y.; Holm, J.; Hansen, S. I.; Jacobsen, C.; Christensen, E. I.; Moestrup, S. K. Megalin Binds and Mediates Cellular Internalization of Folate Binding Protein. *FEBS J.* **2005**, *272*, 4423−4430.
(91) Christensen, E. I.; Birn, H. Megalin and Cubilin: Multifunctional Endocytic Receptors. *Nat. Rev. Mol. Cell Biol.* **2002**, *3*, 258−268.
(92) Rothberg, K. G.; Ying, Y. S.; Kolhouse, J. F.; Kamen, B. A.; Anderson, R. G. The Glycophospholipid-Linked Folate Receptor Internalizes Folate without Entering the Clathrin-Coated Pit Endocytic Pathway. *J. Cell Biol.* **1990**, *110*, 637.
(93) Rothberg, K. G.; Ying, Y. S.; Kamen, B. A.; Anderson, R. G. Cholesterol Controls the Clustering of the Glycophospholipid-Anchored Membrane Receptor for 5-Methyltetrahydrofolate. *J. Cell Biol.* **1990**, *111*, 2931.

DOI: 10.1021/acs.biomac.8b00375
Biomacromolecules 2018, 19, 1469−1484

(94) Smart, E. J.; Mineo, C.; Anderson, R. G. W. Clustered Folate Receptors Deliver 5-Methyltetrahydrofolate to Cytoplasm of MA104 Cells. *J. Cell Biol.* **1996**, *134*, 1169−1177.
(95) Moradi, E.; Vllasaliu, D.; Garnett, M.; Falcone, F.; Stolnik, S. Ligand Density and Clustering Effects on Endocytosis of Folate Modified Nanoparticles. *RSC Adv.* **2012**, *2*, 3025.
(96) Weitman, S. D.; Weinberg, A. G.; Coney, L. R.; Zurawski, V. R.; Jennings, D. S.; Kamen, B. A. Cellular Localization of the Folate Receptor: Potential Role in Drug Toxicity and Folate Homeostasis. *Cancer Res.* **1992**, *52*, 6708−6711.
(97) Campbell, I. G.; Jones, T. A.; Foulkes, W. D.; Trowsdale, J. Folate-Binding Protein Is a Marker for Ovarian Cancer Folate-Binding Protein Is a Marker for Ovarian Cancer. *Cancer Res.* **1991**, *51*, 5329−5338.
(98) Weitman, S. D.; Lark, R. H.; Coney, L. R.; Fort, D. W.; Frasca, V.; Zurawski, V. R.; Kamen, B. A. Distribution of the Folate Receptor GP38 in Normal and Malignant Cell Lines and Tissues. *Cancer Res.* **1992**, *52*, 3396−3401.
(99) Ross, J. F.; Chaudhuri, P. K.; Ratnam, M. Differential Regulation of Folate Receptor Isoforms in Normal and Malignant Tissues in Vivo and in Established Cell Lines. Physiologic and Clinical Implications. *Cancer* **1994**, *73*, 2432−2443.
(100) Bandara, N. A.; Hansen, M. J.; Low, P. S. Effect of Receptor Occupancy on Folate Receptor Internalization. *Mol. Pharmaceutics* **2014**, *11*, 1007−1013.
(101) Sega, E.; Low, P. Tumor Detection Using Folate Receptor-Targeted Imaging Agents. *Cancer Metastasis Rev.* **2008**, *27*, 655−664.
(102) Hilgenbrink, A. R.; Low, P. S. Folate Receptor-Mediated Drug Targeting: From Therapeutics to Diagnostics. *J. Pharm. Sci.* **2005**, *94*, 2135−2146.
(103) Bailey, L. B.; Gregory, J. F. Folate Metabolism and Requirements. *J. Nutr.* **1999**, *129*, 779−782.
(104) Kompis, I. M.; Islam, K.; Then, R. L. DNA and RNA Synthesis: Antifolates. *Chem. Rev.* **2005**, *105*, 593−620.
(105) Chen, C.; Ke, J.; Zhou, X. E.; Yi, W.; Brunzelle, J. S.; Li, J.; Yong, E.-L.; Xu, H. E.; Melcher, K. Structural Basis for Molecular Recognition of Folic Acid by Folate Receptors. *Nature* **2013**, *500*, 486−489.
(106) Wibowo, A. S.; Singh, M.; Reeder, K. M.; Carter, J. J.; Kovach, A. R.; Meng, W.; Ratnam, M.; Zhang, F.; Dann, C. E. Structures of Human Folate Receptors Reveal Biological Trafficking States and Diversity in Folate and Antifolate Recognition. *Proc. Natl. Acad. Sci. U. S. A.* **2013**, *110*, 15180−15188.
(107) Low, P. S.; Henne, W. A.; Doorneweerd, D. D. Discovery and Development of Folic-Acid-Based Receptor Targeting for Imaging and Therapy of Cancer and Inflammatory Diseases. *Acc. Chem. Res.* **2008**, *41*, 120−129.
(108) Low, P. S.; Kularatne, S. A. Folate-Targeted Therapeutic and Imaging Agents for Cancer. *Curr. Opin. Chem. Biol.* **2009**, *13*, 256−262.
(109) Leamon, C. P.; Reddy, J. A. Folate-Targeted Chemotherapy. *Adv. Drug Delivery Rev.* **2004**, *56*, 1127−1141.
(110) Assaraf, Y. G.; Leamon, C. P.; Reddy, J. A. The Folate Receptor as a Rational Therapeutic Target for Personalized Cancer Treatment. *Drug Resist. Updates* **2014**, *17*, 89.
(111) Sudimack, J.; Lee, R. J. Targeted Drug Delivery via the Folate Receptor. *Adv. Drug Delivery Rev.* **2000**, *41*, 147−162.
(112) Wu, Y.; Guo, R.; Wen, S.; Shen, M.; Zhu, M.; Wang, J.; Shi, X. Folic Acid-Modified Laponite Nanodisks for Targeted Anticancer Drug Delivery. *J. Mater. Chem. B* **2014**, *2*, 7410−7418.
(113) Hu, Y.; Wang, R.; Wang, S.; Ding, L.; Li, J.; Luo, Y.; Wang, X.; Shen, M.; Shi, X. Multifunctional Fe_3O_4 @ Au Core/shell Nanostars: A Unique Platform for Multimode Imaging and Photothermal Therapy of Tumors. *Sci. Rep.* **2016**, *6*, 28325.
(114) Cedervall, T.; Lynch, I.; Lindman, S.; Berggård, T.; Thulin, E.; Nilsson, H.; Dawson, K. A.; Linse, S. Understanding the Nanoparticle-Protein Corona Using Methods to Quantify Exchange Rates and Affinities of Proteins for Nanoparticles. *Proc. Natl. Acad. Sci. U. S. A.* **2007**, *104*, 2050−2055.
(115) Lynch, I.; Cedervall, T.; Lundqvist, M.; Cabaleiro-Lago, C.; Linse, S.; Dawson, K. A. The Nanoparticle−protein Complex as a Biological Entity; a Complex Fluids and Surface Science Challenge for the 21st Century. *Adv. Colloid Interface Sci.* **2007**, *134*, 167−174.
(116) Salvati, A.; Åberg, C.; Dawson, K. A.; Monopoli, M. P.; Åberg, C.; Salvati, A.; Dawson, K. A.; Aberg, C.; Salvati, A.; Dawson, K. A. Biomolecular Coronas Provide the Biological Identity of Nanosized Materials. *Nat. Nanotechnol.* **2012**, *7*, 779−786.
(117) Aggarwal, P.; Hall, J. B.; McLeland, C. B.; Dobrovolskaia, M. A.; McNeil, S. E. Nanoparticle Interaction with Plasma Proteins as It Relates to Particle Biodistribution, Biocompatibility and Therapeutic Efficacy. *Adv. Drug Delivery Rev.* **2009**, *61*, 428−437.
(118) Owens, D. E., III; Peppas, N. A. Opsonization, Biodistribution, and Pharmacokinetics of Polymeric Nanoparticles. *Int. J. Pharm.* **2006**, *307*, 93−102.
(119) Walczyk, D.; Bombelli, F. B.; Monopoli, M. P.; Lynch, I.; Dawson, K. A. What the Cell "sees" in Bionanoscience. *J. Am. Chem. Soc.* **2010**, *132*, 5761−5768.
(120) Lynch, I.; Dawson, K. A. Protein-Nanoparticle Interactions. *Nano Today* **2008**, *3*, 40−47.
(121) Antony, A. C. Folate Receptors. *Annu. Rev. Nutr.* **1996**, *16*, 501−521.
(122) Matherly, L. H.; Hou, Z.; Deng, Y. Human Reduced Folate Carrier: Translation of Basic Biology to Cancer Etiology and Therapy. *Cancer Metastasis Rev.* **2007**, *26*, 111−128.
(123) Otsuka, H.; Nagasaki, Y.; Kataoka, K. PEGylated Nanoparticles for Biological and Pharmaceutical Applications. *Adv. Drug Delivery Rev.* **2003**, *55*, 403−419.
(124) Starpharama − VivaGel®. http://www.starpharma.com/vivagel (accessed April 4, 2018).
(125) Kratz, F.; Elsadek, B. Clinical Impact of Serum Proteins on Drug Delivery. *J. Controlled Release* **2012**, *161*, 429−445.
(126) Elsadek, B.; Kratz, F. Impact of Albumin on Drug Delivery — New Applications on the Horizon. *J. Controlled Release* **2012**, *157*, 4−28.
(127) Kratz, F. Albumin as a Drug Carrier: Design of Prodrugs, Drug Conjugates and Nanoparticles. *J. Controlled Release* **2008**, *132*, 171−183.
(128) Merlot, A. M.; Kalinowski, D. S.; Richardson, D. R. Unraveling the Mysteries of Serum Albumin - More than Just a Serum Protein. *Front. Physiol.* **2014**, *5*, 1−7.
(129) Larsen, M. T.; Kuhlmann, M.; Hvam, M. L.; Howard, K. A. Albumin-Based Drug Delivery: Harnessing Nature to Cure Disease. *Mol. Cell. Ther.* **2016**, *4*, 3.
(130) Zhu, G.; Lynn, G. M.; Jacobson, O.; Chen, K.; Liu, Y.; Zhang, H.; Ma, Y.; Zhang, F.; Tian, R.; Ni, Q.; et al. Albumin/vaccine Nanocomplexes That Assemble in Vivo for Combination Cancer Immunotherapy. *Nat. Commun.* **2017**, *8*, 1954.
(131) Chiti, F.; Dobson, C. M. Amyloid Formation by Globular Proteins under Native Conditions. *Nat. Chem. Biol.* **2009**, *5*, 15−22.

DOI: 10.1021/acs.biomac.8b00375
Biomacromolecules 2018, 19, 1469−1484